Mountain View, CA, USA) and that in tissues was carried out by non-compartmental analysis. The elimination rate constant (k_{el}) was estimated by the least square method from the terminal phase. The elimination half-life ($t_{1/2}$) was calculated using the following equation.

$$t_{1/2} = \frac{\ln 2}{k_{el}}$$

Area under concentration *versus* time curve ($AUC_{0\to\infty}$), area under moment curve ($AUMC_{0\to\infty}$), and mean residence time (MRT) were estimated using a trapezoid formula from 0 h to the last measurement time (T), after which the last observed concentration (C_T) and $t_{1/2}$ were used as follows:

$$AUC_{0\to\infty} = \int_0^T C\,dt + \frac{C_T}{k_{el}}$$
$$AUMC_{0\to\infty} = \int_0^T t \cdot C\,dt + \frac{T \cdot C_T}{k_{el}} = \frac{C_T}{k_{el}^2}$$
$$MRT = \frac{AUMC_{0\to\infty}}{AUC_{0\to\infty}}$$

where C is the observed plasma or tissue concentration (plasma: ng/mL, tissues: ng/g skin) and t equals the measurement time (h).

Statistical Analysis

For statistical comparisons, a one-way analysis of variance (ANOVA) with pairwise comparison by the Fisher's least significant difference procedure was used. A p value of less than 0.05 was considered significant for all analyses.

RESULTS AND DISCUSSION

Photostability Testing on Pirfenidone Formulations

The photochemical reactivity of a drug formulation, as well as its chemical stability, is an important aspect to consider during development, production, storage, and use of pharmaceutical preparations. PFD is a potent UV absorber with a molar extinction coefficient of 6,450 $M^{-1}.cm^{-1}$ (λ_{max}: 313 nm, data not shown) and may be photolabile when it absorbed the photon energy, possibly leading to a loss in its potency. Therefore, in the present study, the photoreactivity of PFD was firstly assessed by a reactive oxygen species (ROS) assay as previously reported by Onoue and Tsuda (15). The ROS assay was established to monitor the generation of ROS, such as singlet oxygen and superoxide, from photoirradiated chemicals (15,17), and ROS generation would be indicative of the photochemical reactivity of tested chemicals (11). Sulisobenzone, a potent UV absorber, has no ability to generate ROS when exposed to simulated sunlight (250 W/m^2; Fig. 1a); therefore, sulisobenzone can be identified to be less photoreactive as reported previously. In contrast, 8-methoxypsoralen (MOP), a known phototoxic and photoreactive chemical, and PFD exhibited potent ROS generation under light exposure. Although 8-MOP slightly exceeded PFD in ROS generation, both chemicals were identified to be photoreactive according to the previously defined threshold [singlet oxygen ($\Delta A_{440\ nm}\ 10^3$): 25; superoxide ($\Delta A_{560\ nm}\ 10^3$): 20] (17,18). From these findings, taken together with observed phototoxicity, PFD would be photoreactive, which raises concerns about its photostability.

In respirable formulation systems, an aerosol of PFD can be produced from both liquid and powder formulations in theory, while the photostability of PFD may limit a viable dosage option. To clarify the photochemical properties in more detail, photostability testing was carried out for powder and liquid forms of PFD using a solar simulator equipped with a Xe lamp (Fig. 1b). None of the PFD samples tested here showed any degradation in chromatographic analysis when they were stored at 25°C for at least 1 h under light protection (data not shown). Exposure of PFD solution to simulated sunlight (250 W/m^2) resulted in the gradual degradation of PFD, and it was likely to follow first-order kinetics with an apparent first-order degradation rate of $0.31\pm0.03\ h^{-1}$. In contrast, no significant degradation was observed in PFD powder under the same irradiation conditions. In general, as previously observed in curcumin (19) and coenzyme Q_{10} (20), photosensitive chemicals in a solution state were far more prone to photodegradation than solid samples due to the high permeability of light and increased mobility of photochemically excited molecules and reactive species. On the basis of the photochemical properties of PFD, taken together with previous findings, a nebulizer system using the liquid formulation of PFD may not be suitable for inhalation therapy with PFD from a stability point of view. This could be a rationale for the development of a PFD-loaded RP formulation (PDF-RP), a dry powder inhaler system, in the present investigation.

Respirable Powder Formulation of Pirfenidone

PFD powders were grinded with lactose by the jet-milling system, and then, PFD-RP, a respirable powder formulation of PFD, was obtained by mixing jet-milled PFD particles and Respitose®, a lactose carrier for inhalation therapy. When PFD-RP was exposed to simulated sunlight (250 W/m^2) (Fig. 1b), PFD-RP was found to be stable for at least 1 h, as observed in powder PFD. Thus, an RP approach would surpass the nebulizer system in terms of photochemical stability; therefore, the formulation strategy may be an appropriate delivery option for PFD to treat IPF. However, because of the photoreactive potential of PFD, appropriate UV-light protection may be necessary for the PFD-RP to maintain product quality during long-term storage.

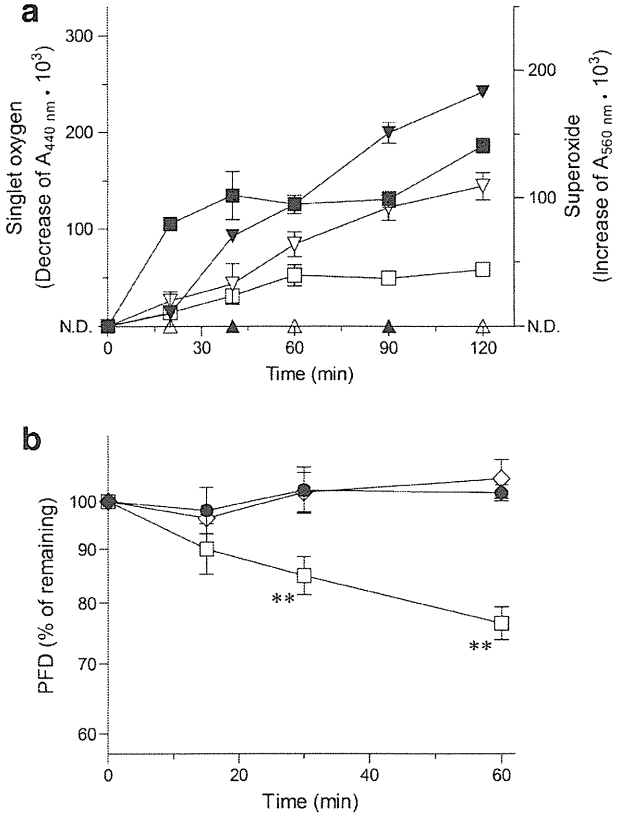

Fig. 1 Photochemical properties of PFD samples. (**a**) Generation of singlet oxygen (*open symbols*) and superoxide (*filled symbols*) from PFD exposed to simulated sunlight (250 W/m^2). □/■, PFD; ▽/▼, 8-MOP; and △/▲, sulisobenzone. Data represent mean±SD of three experiments. (**b**) Photostability data on PFD formulations under exposure to simulated sunlight (250 W/m^2). □, PFD solution; ◇, PFD powder; and ●, PFD-RP. Data represent mean±SD of three experiments. **, $P<0.01$ with respect to the PFD powder.

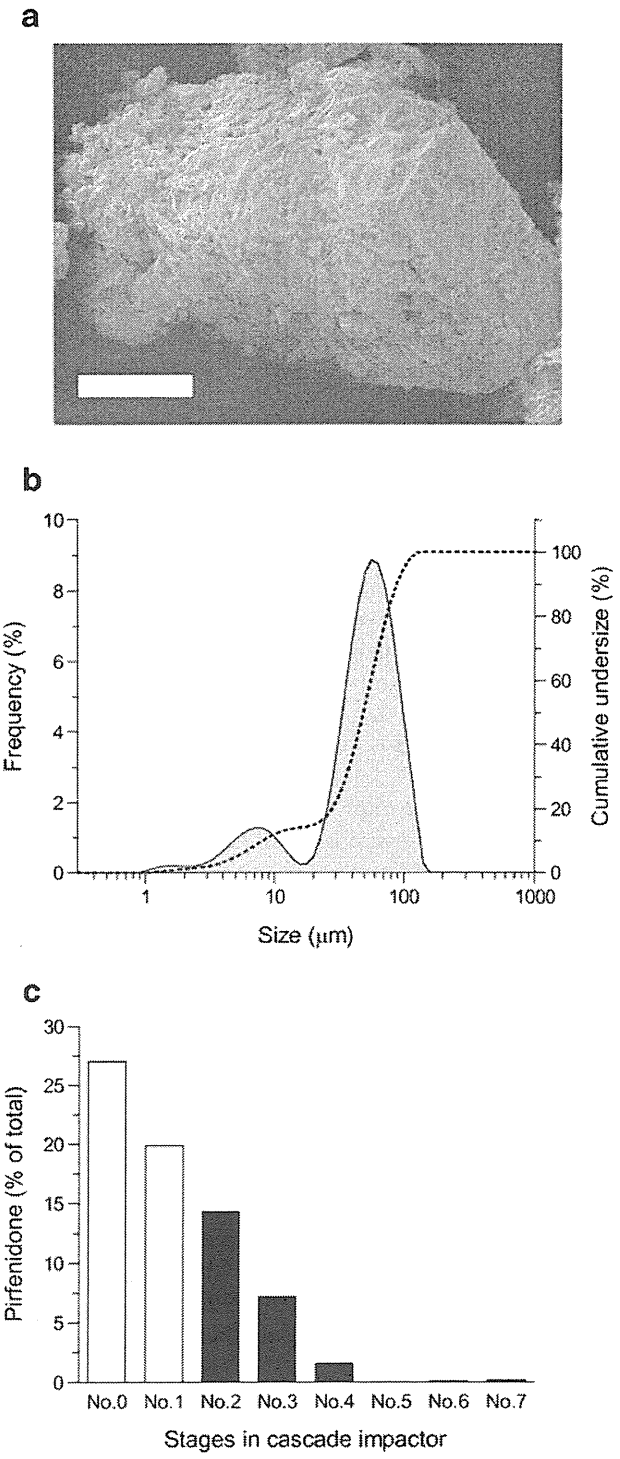

Fig. 2 Appearance and aerosolization efficiency of PFD-RP. (**a**) Scanning electron microscopic images of PFD-RP. Bar represents 20 μm. (**b**) Particle size and aerosolization efficiency of PFD-RP as determined by laser diffraction particle size analysis. PFD-RP was dispersed by dry air at a pressure of 0.2 MPa. *Solid line*, frequency; and *dotted line*, cumulative undersize fraction curve. (**c**) *In vitro* inhalation performance of PFD-RP. Deposition pattern analysis of PFD-RP was conducted using a cascade impactor connecting JetHaler® with an airflow rate of 28.3 L/min.

For better clinical outcomes from inhalation therapy, micronized particles in the RP formulation should be well aerosolized and delivered into respiratory systems. In particular, particle size and the dispersibility of inhalable particles could be key factors when deeply inhaled into the lung and for achieving favorable effects on pulmonary diseases (21). In this context, the physicochemical properties of PFD-RP were assessed with a focus on surface morphology, particle size distribution, and *in vitro* inhalation performance (Fig. 2). The surface morphology of PFD-RP was visualized by SEM (Fig. 2a), demonstrating that micronized PFD particles could be obtained in the form of uniform spherical particles by jet-milling and micronized particles were attached to the surface of lactose carriers without any significant agglomeration. In the laser diffraction analysis of PFD-RP (Fig. 2b) dispersed with pressuring air at 2.0 kg/cm^{2}G, there appeared to be two clear peaks for jet-milled PFD particles and carriers at ca. 7 and ca. 65 μm, respectively. This data suggested the fine dispersion and aerosolization of jet-milled PFD powders under the

experimental condition and that jet-milled PFD particles may be micronized well with a mean diameter of ca. 7.0 μm and a SPAN factor of ca. 1.4. The size of a drug particle critically influences lung deposition (22), and the nature of the aerosolized particles is dependent on its mass median aerodynamic diameter (MMAD) that is a function of particle size, shape and density. Aerosols should be neither too large nor too small. According to a previous report (23), the optimal particle size of drugs to achieve a fine delivery to the bronchial tubes and alveolus was ca. 3–9 μm. Inhaled particles with diameter of over 10 μm, such as carrier particles, are deposited in the mouth or oropharynx, being eventually absorbed from the gut. Particles with diameter of less than 0.5 μm can be inhaled into the deep lung but have a high probability of being exhaled before deposition. In this context, the jet-milled PFD particles with mean diameter of ca. 7.0 μm would be delivered to the pulmonary tissues, possibly leading to the topical therapeutic effects, although the carrier particles might be deposited in the mouth. Therefore, the prepared PFD-RP could be theoretically appropriate for inhalation use. The *in vitro* inhalation performance of PFD-RP was further characterized by cascade impactor analysis (Fig. 2c), in which a JetHaler® inhalation device was employed for drug-carrier separation and fine aerosolization. The emitted dose of PFD-RP from capsules and the FPF value were calculated to be 98.6% and 23.4%, respectively. However, ca. 56% of this still remained in the inhalation device or was deposited in the impactor throat and ca. 20% of PFD was deposited in stages 0 and 1. From these physicochemical data, PFD-RP would have an adequate *in vitro* inhalation performance, although further optimization of RP formulation may still be achievable.

Anti-inflammatory Effect on Antigen-evoked Airway Inflammatory Animal Model

In patients with IPF, a significant increase in BAL neutrophils has been noted in 70–90% of patients and the presence of BAL neutrophilia increases the likelihood of underlying fibrotic processes (24). Previously, Beeh and co-workers also demonstrated the established role of neutrophilic inflammation in the pathogenesis of IPF (25). In the present study, to elucidate the therapeutic potential of PFD-RP, the anti-inflammatory effects of insufflated PFD-RP in the respiratory system were assessed using airway inflammatory rats, in which the RP formulation of OVA, an antigen, induced topical inflammatory events in the lung, such as severe neutrophilia and weak eosinophilia (16). At 24 h after antigen insufflation, BALF was obtained to monitor the recruitment of inflammatory cells in the lung (Fig. 3a), since BALF has been frequently used as a biological source for clinical investigation of inflammatory lung diseases (26). Insufflated OVA, an antigen, caused marked recruitment of inflammatory cells in BALF as evidenced by a 6.5-fold increase in total cell numbers, mainly

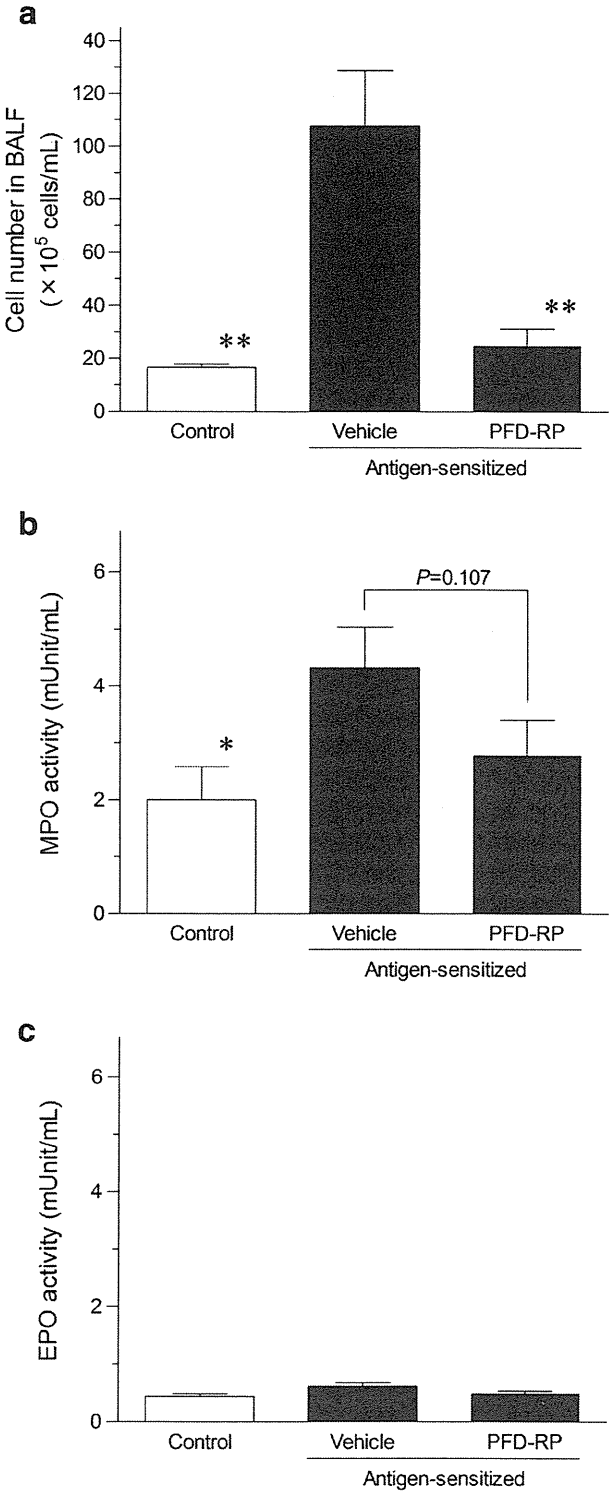

Fig. 3 Anti-inflammatory effects of inhaled PFD-RP in antigen-sensitized rats. At 24 h after the antigen challenge, (**a**) recruited inflammatory cells, (**b**) MPO levels, or (**c**) EPO levels in BALF were monitored in rats with or without pretreatment of PFD-RP (300 μg-PFD/kg). Data represent the mean±SE of 4–6 determinations. *, $P<0.05$ and **, $P<0.01$ with respect to antigen-sensitized rats with inhaled control-RP.

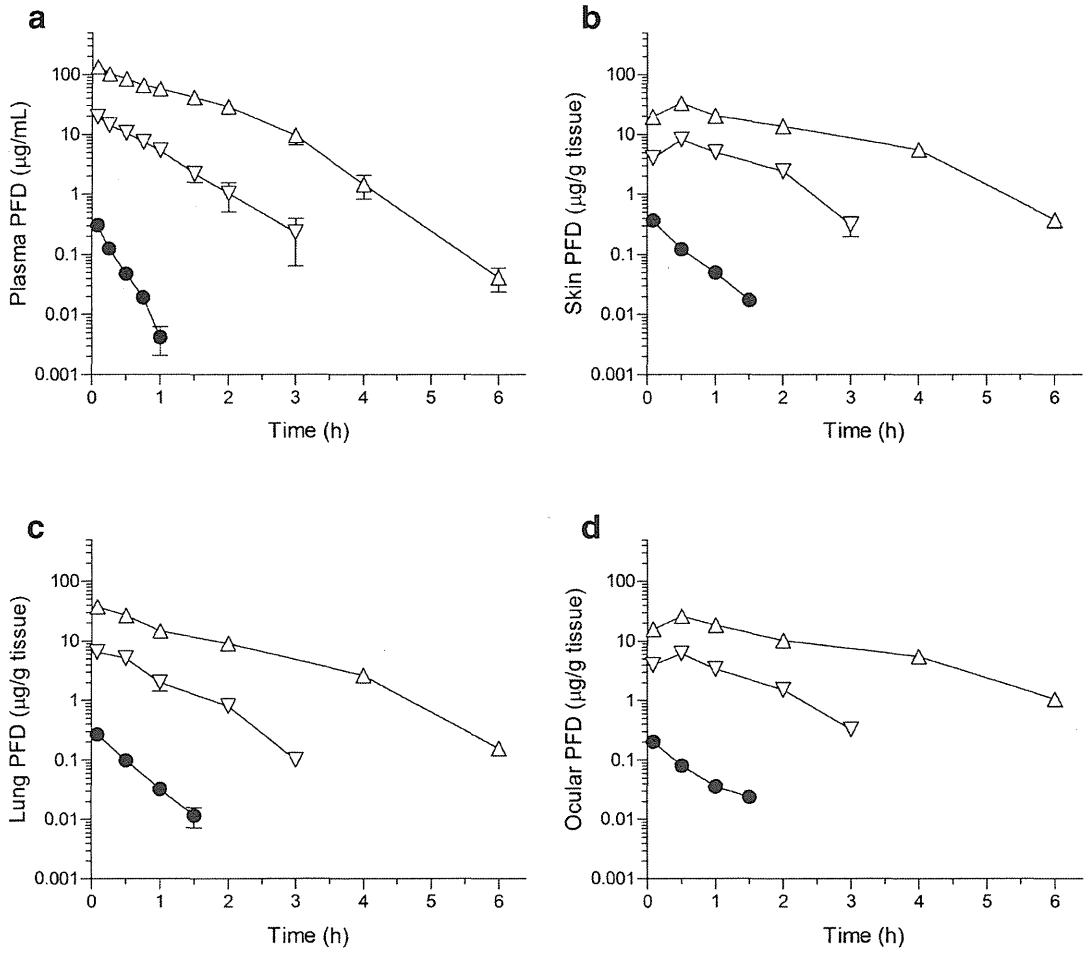

Fig. 4 Concentration-time profiles of PFD in plasma (**a**), skin (**b**), lung (**c**), and eyes (**d**) after intratracheal administration of PFD-RP and oral administration of PFD in rats. ●, insufflated PFD-RP at a pharmacologically effective dose (300 μg PFD/rat); △, orally-taken PFD at a phototoxic dose (160 mg/kg); and ▽, at a non-phototoxic dose (30 mg/kg). Each value represents mean±SE for 4–8 determinations.

consisting of monocytes and neutrophils. In contrast, antigen-evoked airway inflammation seemed to be significantly attenuated by pretreatment with PFD-RP (30–1,000 μg of PFD/rat) in a dose-dependent manner, although PFD-RP at a dose of 100 μg of PFD/rat or lower was found to be less effective. In particular, there appeared to be ca. 90% reduction in infiltrated cells in BALF from sensitized-rats with pretreatment of PFD-RP (300 μg of PFD/rat), and the efficacy of PFD-RP at dose of 1,000 μg-PFD/rat was almost identical to that at 300 μg of PFD/rat in the present experimental model (data not shown). There were no significant differences in the number of recruited cells in BALF between control and antigen-exposed rats with pretreatment of PFD-RP at dose of 300 μg of PFD/rat or much higher. These data were indicative of the therapeutic potential of PFD-RP against airway inflammation and the early symptoms of IPF.

In the development of airway inflammation and fibrotic diseases, MPO and EPO sometimes act as pro-inflammatory and pro-oxidant mediators, mainly released from activated neutrophils/macrophages and eosinophils, respectively (27). These enzymatic activities in BALF have thus been recognized as biomarkers for neutrophilia and eosinophilia. At 24 h after the last antigen challenge, MPO activity in BALF was markedly increased after the OVA challenge (Fig. 3b; 2.00±0.58 and 4.32±0.71 mUnit/mL in non-sensitized and OVA-sensitized rats, respectively), whereas no significant elevations in EPO levels in BALF were seen (Fig. 3c; 0.44±0.05 and 0.62±0.06 mUnit/mL in non-sensitized and OVA-sensitized rats, respectively). From these data, an antigen challenge in the airway system resulted in significant elevations in MPO levels in the lung, suggesting the development of pulmonary neutrophilia in OVA-exposed rats. Pretreatment with PFD-RP (300 μg of PFD/rat) tended to attenuate up-regulation of MPO levels in BALF of OVA-exposed rats by 67%. Not surprisingly, no significant changes in EPO levels were seen even after pre-

treatment with PFD-RP at same dose. Thus, insufflated PFD-RP would be efficacious for suppression of neutrophilic inflammatory symptoms. These observations were in agreement with the inhibitory effects of PFD-RP on the recruitment of inflammatory cells in BALF and the present data could also be indicative of the topical therapeutic potential of PFD-RP for the treatment of pulmonary inflammatory and fibrotic diseases.

In general, localized targeted delivery of drugs into the lungs would offer two primary benefits: (i) reduced nominal dose, which lowers the cost of goods, and (ii) reduced off-target drug exposure, possibly leading to lower systemic side-effects. Previous investigations demonstrated the high therapeutic potential of PFD in several experimental animal models of pulmonary fibrosis, including the anti-fibrotic activity of PFD (p.o., 30 or 100 mg/kg/day) in the bleomycin model of pulmonary fibrosis and the anti-inflammatory effects of PFD (s.c., 500 mg/kg) in an antigen-sensitized model. For the clinical treatment of IPF, PFD was administered orally three times per day with meals, in a total daily dose of 1.8 g, corresponding to ca. 30 mg/kg. In our animal experiments, a pharmacologically effective dose for the RP formulation was deduced to be 300 μg of PFD/rat (ca. 1 mg/kg); however, PFD in systemic administration was found to be effective only at much higher doses. Although a simple and direct comparison on these doses may not be appropriate because of inconsistent experimental conditions, the RP formulation approach would result in marked reductions in the dose of PFD needed to achieve topical pharmacological effects in the lungs.

Pharmacokinetic Behaviour of Pirfenidone after Oral or Intratracheal Administration

From the pharmacological outcomes, reductions in the nominal dose of PFD can be achieved upon the RP formulation strategy; however, de-risk of the phototoxic potential is still unclear. In general, since drug-induced phototoxic responses appear in the skin and eyes, the specific distribution of drug molecules in the skin and/or eyes could be a key consideration for evaluating the phototoxic risk. In the present study, to verify the photosafety of PFD-RP, a pharmacokinetic study on PFD was undertaken after intratracheal administration of PFD-RP at a pharmacologically effective dose (300 μg-PFD/rat). In addition, on the basis of previous findings on phototoxic (160 mg/kg) and non-phototoxic (30 mg/kg) doses in rats (28), pharmacokinetic behaviors of PFD were also characterized after oral administration of a PFD suspension at both doses (30 and 160 mg/kg) for comparison. Concentration-time curves of PFD in the plasma, skin, lung, and eyes were obtained by UPLC/ESI-MS analysis after intratracheal and oral administrations (Fig. 4), and relevant pharmacokinetic parameters of PFD, including C_{max}, $t_{1/2}$, $AUC_{0\to\infty}$, and MRT, were summarized in Table I. After oral administration of PFD, plasma and lung concentrations of PFD immediately reached the C_{max} within 5 min and these concentrations decreased steadily with half lives of ca. 0.3–0.8 h. With respect to skin and eye depositions, delayed distribution phases were observed, reaching maximum levels at ca. 0.5 h after oral dosing, followed by an elimination phase with a half-life of ca. 0.7–1.1 h. Thus, the elimination of PFD from the skin and eyes was found to

Table I PK Parameters of Plasma and Tissues on PFD in Rats After Oral and Intratracheal Administrations

Samples	C_{max} (plasma, μg/mL; tissues, μg/g tissue)	$t_{1/2}$ (h)	$AUC_{0\to\infty}$ (plasma, h•μg/mL; tissues, h•μg/g tissue)	MRT (h)
Plasma				
PFD-RP (300 μg-PFD/rat, i.t.)	0.307 ± 0.039	0.17 ± 0.02	0.0835 ± 0.011	0.261 ± 0.011
PFD (30 mg/kg, p.o.)	19.7 ± 0.93	0.33 ± 0.02	14.1 ± 0.92	0.667 ± 0.094
PFD (160 mg/kg, p.o.)	135 ± 11	0.53 ± 0.03	152 ± 10	1.05 ± 0.075
Skin				
PFD-RP (300 μg-PFD/rat, i.t.)	0.369 ± 0.014	0.24 ± 0.02	0.183 ± 0.029	0.427 ± 0.0051
PFD (30 mg/kg, p.o.)	8.16 ± 0.47	1.07 ± 0.28	11.5 ± 0.51	1.14 ± 0.12
PFD (160 mg/kg, p.o.)	32.9 ± 2.6	1.06 ± 0.24	68.0 ± 1.4	1.70 ± 0.043
Lung				
PFD-RP (300 μg-PFD/rat, i.t.)	0.271 ± 0.035	0.28 ± 0.08	0.136 ± 0.039	0.421 ± 0.0080
PFD (30 mg/kg, p.o.)	6.46 ± 0.69	0.80 ± 0.24	6.45 ± 0.43	0.787 ± 0.16
PFD (160 mg/kg, p.o.)	37.6 ± 5.7	0.77 ± 0.16	52.1 ± 1.0	1.32 ± 0.041
Eyes				
PFD-RP (300 μg-PFD/rat, i.t.)	0.202 ± 0.019	0.27 ± 0.06	0.120 ± 0.030	0.554 ± 0.0084
PFD (30 mg/kg, p.o.)	3.95 ± 0.30	0.67 ± 0.18	8.33 ± 0.39	1.06 ± 0.13
PFD (160 mg/kg, p.o.)	26.0 ± 2.6	1.06 ± 0.27	58.8 ± 1.3	1.93 ± 0.051

Each parameter was calculated on the basis of concentration-time curves in plasma and tissues. i.t.: intratracheal administration; and p.o.: oral administration. Each value represents mean ± S.E. for 4–8 rats

be slower than that in plasma and PFD may accumulate in these light-exposed areas (skin and eyes) upon chronic dosing, resulting in an increased phototoxic risk. In contrast, after intratracheal administration of PFD-RP at a pharmacologically effective dose (300 μg-PFD/rat), all plasma and tissue concentrations of PFD immediately reached the C_{max} within 5 min, and then, these concentrations rapidly diminished below detectable levels within 1.5 h. According to estimated PK parameters of PFD in plasma and tissues on the basis of concentration-time curves, C_{max} and $AUC_{0\to\infty}$ values in insufflated PFD-RP at a pharmacologically effective dose (300 μg-PFD/rat) were much lower than those in orally-taken PFD at both phototoxic (160 mg/kg) and non-phototoxic doses (30 mg/kg). In particular, compared with orally-taken PFD at the phototoxic dose, insufflated PFD-RP at the pharmacologically effective dose led to ca. 440-, 90-, and 30-fold reductions in C_{max} values for plasma, skin, and eyes, respectively. The reduced systemic exposure of PFD was also confirmed with decreases in $AUC_{0\to\infty}$ values in plasma, skin, and eyes by ca. 1,800-, 370-, and 440-fold, respectively. In addition, there were still ca. 63–70-fold differences in $AUC_{0\to\infty}$ values for skin and ocular PFD between rats treated with insufflated PFD-RP and orally-taken PFD at non-phototoxic doses (30 mg/kg). From these comparative pharmacokinetic studies, compared with PFD for oral use, the application of the RP system to PFD successfully resulted in marked decreases in skin and eye deposition of PFD, as well as systemic exposure.

In our previous study, the phototoxic potential of fluoroquinolones (FQs) was assessed by *in vitro* phototoxicity assays and an *in vivo* pharmacokinetic study (12). Interestingly, even though most FQs exhibited potent *in vitro* phototoxicity through potent ROS generation under light exposure, FQs with low skin distribution properties were found to be less phototoxic *in vivo*. Thus, the photosafety assessment could be made with combined use of photochemical properties and pharmacokinetic behavior, especially deposition on light-exposed areas. From these previous findings, taken together with the present pharmacokinetic data on PFD, moderate skin disposition upon the RP formulation approach would be efficacious for de-risk of PFD-induced phototoxicity by suppressing excess systemic exposure of PFD. The newly developed PFD-RP system may provide an interesting alternative to oral therapy with a better safety margin for the treatment of IPF. However, since the photosafety of chronic use of PFD-RP is still uncertain, further photosafety assessments may be needed before its clinical use. In addition to the phototoxicity, orally-taken PFD sometimes cause hepatic dysfunction and gastrointestinal side effects such as dyspepsia, nausea and gastroesophageal reflux disease (6,8,9). On the basis of the pharmacokinetic data, these other systemic side-effects might also be attenuated by the newly developed PFD-RP system, because of the limited systemic exposure of PFD after its insufflation. In this context, there may be a need for further comparative studies on (i) toxic biomarkers specific for liver dysfunction and/or gastrointestinal side effects, and (ii) distribution of PFD in gastrointestinal tract and liver. The outcomes from these investigations might provide further support for improved safety of the PFD-RP system in the near future.

CONCLUSION

In the present study, an RP formulation of PFD for the treatment of IPF was firstly prepared to improve photosafety and lower the nominal dose. Photostability testing on PFD formulations demonstrated that PFD-RP, as well as PFD powder, was more highly photostable than that of the PFD solution. PFD-RP also exhibited high dispersibility and suitable particle distribution for inhalation therapy. In antigen-sensitized inflammatory-model rats, insufflated PFD-RP could attenuate antigen-evoked inflammatory symptoms and neutrophilia in the lung. Most notably, PFD-RP at a pharmacologically effective dose (300 μg-PFD/rat) could reduce the phototoxic potential of PFD because of its lower systemic exposure and distribution to light-exposed tissues than that after oral administration of PFD at a phototoxic dose (160 mg/kg). From these findings, the PFD-RP system may provide efficacious and safe medication for the clinical treatment of IPF.

ACKNOWLEDGMENTS AND DISCLOSURES

Authors are grateful to Shionogi&Co., Ltd. for kindly providing pirfenidone. This work was supported in part by a Grant-in-Aid for Young Scientists (B) (No. 22790043; S. Onoue) from the Ministry of Education, Culture, Sports, Science, and Technology and a Health Labour Sciences Research Grant from The Ministry of Health, Labour, and Welfare, Japan.

REFERENCES

1. Hisatomi K, Mukae H, Sakamoto N, Ishimatsu Y, Kakugawa T, Hara S, *et al.* Pirfenidone inhibits TGF-ss1-induced over-expression of collagen type I and heat shock protein 47 in A549 cells. BMC Pulm Med. 2012;12:24.
2. Iyer SN, Gurujeyalakshmi G, Giri SN. Effects of pirfenidone on transforming growth factor-beta gene expression at the transcriptional level in bleomycin hamster model of lung fibrosis. J Pharmacol Exp Ther. 1999;291:367–73.
3. Lasky J. Pirfenidone. IDrugs. 2004;7:166–72.
4. Schaefer CJ, Ruhrmund DW, Pan L, Seiwert SD, Kossen K. Antifibrotic activities of pirfenidone in animal models. Eur Respir Rev. 2011;20:85–97.

5. Corbel M, Lanchou J, Germain N, Malledant Y, Boichot E, Lagente V. Modulation of airway remodeling-associated mediators by the antifibrotic compound, pirfenidone, and the matrix metalloproteinase inhibitor, batimastat, during acute lung injury in mice. Eur J Pharmacol. 2001;426:113–21.
6. Hilberg O, Simonsen U, du Bois R, Bendstrup E. Pirfenidone: significant treatment effects in idiopathic pulmonary fibrosis. Clin Respir J. 2012;6:131–43.
7. Richeldi L, Yasothan U, Kirkpatrick P. Pirfenidone. Nat Rev Drug Discov. 2011;10:489–90.
8. Taniguchi H, Ebina M, Kondoh Y, Ogura T, Azuma A, Suga M, *et al.* Pirfenidone in idiopathic pulmonary fibrosis. Eur Respir J. 2010;35:821–9.
9. Carter NJ. Pirfenidone: in idiopathic pulmonary fibrosis. Drugs. 2011;71:1721–1732.
10. Steinand KR, Scheinfeld NS. Drug-induced photoallergic and phototoxic reactions. Expert Opin Drug Saf. 2007;6:431–43.
11. Onoue S, Seto Y, Gandy G, Yamada S. Drug-induced phototoxicity; an early *in vitro* identification of phototoxic potential of new drug entities in drug discovery and development. Curr Drug Saf. 2009;4:123–36.
12. Seto Y, Inoue R, Ochi M, Gandy G, Yamada S, Onoue S. Combined use of *in vitro* phototoxic assessments and cassette dosing pharmacokinetic study for phototoxicity characterization of fluoroquinolones. AAPS J. 2011;13:482–92.
13. Onoue S, Aoki Y, Kawabata Y, Matsui T, Yamamoto K, Sato H, *et al.* Development of inhalable nanocrystalline solid dispersion of tranilast for airway inflammatory diseases. J Pharm Sci. 2011;100:622–33.
14. Onoue S, Sato H, Kawabata Y, Mizumoto T, Hashimoto N, Yamada S. *In vitro* and *in vivo* characterization on amorphous solid dispersion of cyclosporine A for inhalation therapy. J Control Release. 2009;138:16–23.
15. Onoueand S, Tsuda Y. Analytical studies on the prediction of photosensitive/phototoxic potential of pharmaceutical substances. Pharm Res. 2006;23:156–64.
16. Misaka S, Sato H, Yamauchi Y, Onoue S, Yamada S. Novel dry powder formulation of ovalbumin for development of COPD-like animal model: Physicochemical characterization and biomarker profiling in rats. Eur J Pharm Sci. 2009;37:469–76.
17. Onoue S, Kawamura K, Igarashi N, Zhou Y, Fujikawa M, Yamada H, *et al.* Reactive oxygen species assay-based risk assessment of drug-induced phototoxicity: Classification criteria and application to drug candidates. J Pharm Biomed Anal. 2008;47:967–72.
18. Onoue S, Hosoi K, Wakuri S, Iwase Y, Yamamoto T, Matsuoka N *et al.* Establishment and intra-/inter-laboratory validation of a standard protocol of reactive oxygen species assay for chemical photosafety evaluation. J Appl Toxicol:in press (2012). doi:10.1002/jat.2776.
19. Onoue S, Takahashi H, Kawabata Y, Seto Y, Hatanaka J, Timmermann B, *et al.* Formulation design and photochemical studies on nanocrystal solid dispersion of curcumin with improved oral bioavailability. J Pharm Sci. 2010;99:1871–81.
20. Matsudaand Y, Masahara R. Photostability of solid-state ubidecarenone at ordinary and elevated temperatures under exaggerated UV irradiation. J Pharm Sci. 1983;72:1198–203.
21. Onoue S, Hashimoto N, Yamada S. Dry powder inhalation systems for pulmonary delivery of therapeutic peptides and proteins. Expert Opin Ther Patents. 2008;18:429–42.
22. Suarezand S, Hickey AJ. Drug properties affecting aerosol behavior. Respir Care. 2000;45:652–66.
23. Labirisand NR, Dolovich MB. Pulmonary drug delivery. Part I: physiological factors affecting therapeutic effectiveness of aerosolized medications. Br J Clin Pharmacol. 2003;56:588–99.
24. Pesci A, Ricchiuti E, Ruggiero R, De Micheli A. Bronchoalveolar lavage in idiopathic pulmonary fibrosis: what does it tell us? Respir Med. 2010;104 Suppl 1:S70–3.
25. Beeh KM, Beier J, Kornmann O, Buhl R. Neutrophilic inflammation in induced sputum of patients with idiopathic pulmonary fibrosis. Sarcoidosis Vasc Diffuse Lung Dis. 2003;20:138–43.
26. Tzortzaki EG, Tsoumakidou M, Makris D, Siafakas NM. Laboratory markers for COPD in "susceptible" smokers. Clin Chim Acta. 2006;364:124–38.
27. Onoue S, Misaka S, Kawabata Y, Yamada S. New treatments for chronic obstructive pulmonary disease and viable formulation/device options for inhalation therapy. Expert Opin Drug Deliv. 2009;6:793–811.
28. Seto Y, Aoki Y, Inoue R, Kojo Y, Kato M, Onoue S, *et al.* Development of dry powder inhaler system for reducing phototoxic risk. In: Oku N, editor. DDS conference, vol. 20. Shizuoka: Biomedical Research Press; 2011. p. 41–6.

Journal of Photochemistry and Photobiology B: Biology 120 (2013) 44–51

Contents lists available at SciVerse ScienceDirect

Journal of Photochemistry and Photobiology B: Biology

journal homepage: www.elsevier.com/locate/jphotobiol

Photosafety assessments on pirfenidone: Photochemical, photobiological, and pharmacokinetic characterization

Yoshiki Seto [a,1], Ryo Inoue [a], Masashi Kato [a], Shizuo Yamada [a], Satomi Onoue [a,*]

[a] Department of Pharmacokinetics and Pharmacodynamics and Global Center of Excellence (COE) Program, School of Pharmaceutical Sciences, University of Shizuoka, 52-1 Yada, Suruga-ku, Shizuoka 422-8526, Japan

ARTICLE INFO

Article history:
Received 19 September 2012
Received in revised form 16 January 2013
Accepted 16 January 2013
Available online 29 January 2013

Keywords:
Phototoxicity
Pirfenidone
Reactive oxygen species
Pharmacokinetic

ABSTRACT

Pirfenidone (PFD), an idiopathic pulmonary fibrosis drug, has phototoxic risk in clinical use, although its detailed mechanisms for the phototoxicity have never been fully elucidated. In the present study, the photochemical properties and *in vitro* phototoxicity of PFD were evaluated with a focus on ultraviolet absorption, reactive oxygen species (ROS) generation, photodynamic lipid peroxidation, and DNA photocleavage. To clarify the *in vivo* phototoxic behavior of PFD, photoirritation and pharmacokinetic characteristics were also assessed in rats after its oral administration. There was marked generation of singlet oxygen and superoxide from PFD upon exposure to simulated sunlight, suggesting its high photoreactivity and phototoxic potential. Photobiochemical studies demonstrated the potent *in vitro* photoirritation of PFD, but not its photogenotoxic risk. Pharmacokinetic profiling and *in vivo* phototoxicity testing on PFD at a dose of 160 mg/kg suggested that highly concentrated PFD in the skin might cause phototoxic skin reactions in rats, whereas PFD at 30 mg/kg was far less phototoxic, possibly due to the limited skin deposition. From these findings, a high dose of orally administered PFD might cause phototoxic skin responses, possibly via a ROS-mediated photoirritant pathway.

1. Introduction

Drug-induced phototoxicity is elicited by exposure of the skin and/or eyes to topical or systemic administration of pharmaceutical substances, followed by exposure to sunlight, especially ultraviolet (UV) A (320–400 nm) and UVB (290–320 nm) radiation [1]. Several classes of drug become reactive upon exposure to sunlight and cause phototoxic reactions, including photoirritation, photoallergy, and photogenotoxicity [2]. On the basis of the mechanisms of drug-induced phototoxicity, a number of effective *in vitro* phototoxicity assessments were previously developed, such as a UV absorption and a 3T3 neutral red uptake phototoxicity test [3]. In the early phototoxic events, reactive oxygen species (ROS), such as singlet oxygen and superoxide, are reported to be major toxic mediators of phototoxic reactions. Previously, ROS assay was established to evaluate generation of ROS from tested chemicals under exposure to simulated sunlight, allowing prediction of photochemical toxicity [4,5]. In addition to these *in vitro* phototoxicity assessments, combined use of *in vitro* photochemical and phototoxic properties and *in vivo* pharmacokinetic (PK) behaviors was previously proposed as a photosafety screening strategy for predicting the *in vivo* phototoxic potential of compounds [6,7].

Pirfenidone (PFD), 5-methyl-1-phenylpyridin-2-one (Fig. 1), mainly exhibits antifibrotic properties, various mechanisms of which have been reported, including regulation of key fibrotic cytokines and growth factors, inhibition of several inflammatory mediators, attenuation of fibroblast proliferation, differentiation, and related collagen synthesis, and restoration of immune response balance [8]. These beneficial effects of PFD could lead to treatment for fibrotic diseases, such as cardiac, renal, liver, and pulmonary fibrosis [9–12], and it is clinically used for treating idiopathic pulmonary fibrosis [13]. However, systemic side effects of PFD after oral administration were previously reported in clinical trials, such as dermatological and gastrointestinal adverse symptoms [14–16]. In particular, PFD-induced phototoxicity occurred with high frequency (ca. 52%) after oral administration as an adverse event in previous clinical trials [16], and patients are usually advised to avoid exposure to sunlight by using photoprotective clothing and sunscreens. Although the phototoxicity of PFD would be a major issue for clinical use, the mechanisms of PFD-induced phototoxicity have not been fully elucidated.

The present study mainly aimed to clarify the detailed mechanisms of phototoxic skin reaction after oral administration of PFD. Photochemical characterization of PFD was carried out by UV absorption and ROS assay to evaluate the photoreactivity of

* Corresponding author. Tel.: +81 54 264 5633; fax: +81 54 264 5635.
E-mail address: onoue@u-shizuoka-ken.ac.jp (S. Onoue).
[1] Current address: Pharmacokinetics and Safety Research Department, Central Research Laboratories, Kaken Pharmaceutical Co. Ltd., 301 Gensuke, Fujieda-shi, Shizuoka 426-8646, Japan.

1011-1344/$ - see front matter © 2013 Elsevier B.V. All rights reserved.
http://dx.doi.org/10.1016/j.jphotobiol.2013.01.010

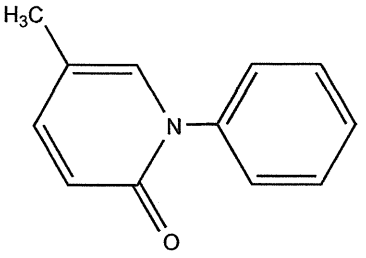

Fig. 1. Chemical structure of PFD.

PFD, possibly relating to phototoxic potentials. Then, the *in vitro* phototoxic properties of PFD were assessed on the basis of photodynamic lipid peroxidation and DNA impairment by irradiated PFD to explore possible mechanisms of PFD-induced phototoxicity. To verify the induction of phototoxic skin reaction by PFD in rats, an *in vivo* phototoxicity test using a colorimeter was also conducted after oral administration of PFD. The PK study after oral administration of PFD was also undertaken with a focus on tissue distribution properties, especially the skin deposition, since the phototoxic reaction would occur in the skin.

2. Materials and methods

2.1. Chemicals

PFD was kindly provided by Shionogi and Co. Ltd. (Osaka, Japan). Butylated hydroxytoluene (BHT), erythromycin (ETM), imidazole, ketoprofen (KPF), nitroblue tetrazolium (NBT), *p*-nitrosodimethylaniline (RNO), plasmid pBR322 DNA, salmon sperm DNA, 1,1,3,3-tetraethoxypropane, thiobarbituric acid (TBA), thiazole orange (TO), Tween 20, disodium hydrogen phosphate 12-hydrate, and sodium dihydrogen phosphate dihydrate were obtained from Wako Pure Chemical Industries (Osaka, Japan). Agarose L03 was purchased from Takara Bio (Shiga, Japan) and ethidium bromide (EtBr) was purchased from Nippon Gene (Toyama, Japan). Acetonitrile (ACN) and methanol were obtained from Kanto Chemical Co. Inc. (Tokyo, Japan).

2.2. UV spectral analysis

PFD was dissolved in 20 mM sodium phosphate buffer (NaPB, pH 7.4) at a final concentration of 20 μM. UV–VIS absorption spectra were recorded with a HITACHI U-2010 spectrophotometer (HITACHI, Tokyo, Japan) interfaced to a PC for data processing (software: Spectra Manager). A spectrofluorimeter quartz cell with 10 mm pathlength was employed.

2.3. Irradiation conditions

Chemicals were stored in an Atlas Suntest CPS + solar simulator (Atlas Material Technology LLC, Chicago, USA) equipped with a xenon arc lamp (1500 W). A UV special filter and a window glass filter were installed to adapt the spectrum of the artificial light source to natural daylight. The irradiation test was carried out at 25 °C with irradiance of 250 W/m^2.

2.4. Determination of reactive oxygen species (ROS)

Both singlet oxygen and superoxide generated from irradiated PFD (20, 50, 100, 200 and 400 μM), KPF (200 μM) and ETM (200 μM) were measured as we reported previously [4]. Briefly, to monitor the generation of singlet oxygen, samples containing the compounds under examination, RNO (50 μM) and imidazole (50 μM) in 20 mM NaPB (pH 7.4), were irradiated with UVA/B, and then the UV absorption at 440 nm was measured using SAFIRE (TECAN, Männedorf, Switzerland). For the determination of superoxide, samples containing the compounds under examination and NBT (50 μM) in 20 mM NaPB (pH 7.4) were irradiated with UVA/B, and the reduction of NBT was measured by the increase in the absorbance at 560 nm using SAFIRE.

2.5. Photosensitized peroxidation of linoleic acid

Linoleic acid (1 mM) suspended in 20 mM NaPB (pH 7.4) containing 0.05% Tween 20 was irradiated in the presence of PFD (100, 200 and 400 μM), KPF (200 μM) and ETM (200 μM), and lipid peroxidation was measured using a TBA assay as described previously [17]. Addition of 0.67% TBA dissolved in 20 mM NaPB (pH 7.4, 1 mL) and 10 μL of 1.0% BHT solution in glacial acetic acid to the irradiated sample (500 μL) was followed by heating at 95 °C for 30 min. The mixture was extracted with 1.0 mL of 1-butanol, and absorbance of the extract was measured at 532 nm for the determination of TBA-reactive substances (TBARS). A standard curve of 1,1,3,3-tetraethoxypropane was used to quantitate the amount of malondialdehyde produced.

2.6. Intercalator-based phototoxicity (IBP) assay

The photodynamic impairment of salmon sperm DNA by PFD (100, 200 and 400 μM), KPF (200 μM) and ETM (200 μM) was evaluated by IBP assay. Each assay mixture (100 μL) in the 96-well microplate, containing compounds and DNA (20 μg/mL) in 20 mM NaPB (pH 7.4), was irradiated with UVA/B for 45 min, and then TO was added to each well at a final concentration of 1.3 μM. As a control experiment, only 80 μL of chemicals in 20 mM NaPB (pH 7.4) was exposed to UVA/B, and then DNA (10 μg/mL) and TO (1.3 μM) were added to the sample. The control experiment gives intercalation properties of photodegradants. In both irradiation and control experiments, each assay mixture (200 μL) was incubated at 37 °C for 15 min to equilibrate intercalation of DNA with TO. To detect the intercalated TO, fluorescence (excitation: 509 nm and emission: 527 nm) was measured with SAFIRE. Each fluorescence data was divided by mean value for vehicle group.

2.7. Agarose gel electrophoresis (AGE)-based photogenotoxicity test

The photodynamic impairment of plasmid DNA by PFD (100, 200 and 400 μM), KPF (200 μM) and ETM (200 μM) was also evaluated by AGE-based photogenotoxicity test. The irradiated samples contained pBR322 DNA (final concentration, 10 μg/mL) dissolved in Tris–acetate-EDTA (TAE) buffer (40 mM Tris, 20 mM boric acid, and 1 mM EDTA; pH 7.4) and the examined compounds. Irradiated plasmid pBR322 DNA was separated by electrophoresis (0.8% agarose gel in TAE buffer), stained with EtBr solution (0.5 μg/mL), and analyzed with image analyzing software Image J.

2.8. In vivo preparations

Male Sprague–Dawley rats at 7–9 weeks of age (ca. 200–350 g, body weight) were purchased from SLC Inc. (Hamamatsu, Japan) and housed in the laboratory with free access to food and water, and maintained on a 12 h dark/light cycle in a room with controlled temperature (24 ± 1 °C) and humidity (55 ± 5%). All the procedures used in the present study were conducted according to the guidelines approved by the Institutional Animal Care and Ethical Committee of the University of Shizuoka.

PFD was dissolved in water containing 0.05% Tween 20. Rats were fasted for approximately 18 h before drug administration, and PFD was orally administered (30, 160 mg/kg).

2.9. In vivo phototoxicity test

Rats were anesthetized using pentobarbital (30 mg/kg), and then the hair on the back was shaved. PFD (30 and 160 mg/kg) was orally administered to rats after awaking from anesthesia, and then the rats were immediately irradiated by black light (FL15BL-B, National, Tokyo, Japan) until the UV irradiance level reached 30 J/cm^2. UV intensity was monitored using a UV-Meter (Dr. Honle AG, UV-technology, Munich, Germany).

A colorimeter equipped with a data processor (NF333, Nippon denshoku, Tokyo, Japan) was used as a measure of skin color. The instrument records three-dimensional color reflectance, the so-called $L^*a^*b^*$ system, as recommended by the Commission Internationale de l'Eclairage (CIE). The luminance (L^*) gives the relative brightness ranging from total black ($L^* = 0$) to total white ($L^* = 100$). The hue (a^*) axis represents the balance between red (positive values up to 100) and green (negative values up to −100), and the chroma (b^*) axis represents the balance between yellow (positive values up to 100) and blue (negative values up to −100). The differences in color (ΔE) between before and after irradiation of the skin were described as follows [18,19]:

$$\Delta E = \sqrt{\{(\Delta L^*)^2 + (\Delta a^*)^2 + (\Delta b^*)^2\}}$$

2.10. Plasma concentration of PFD after oral administration

Rats were anesthetized using pentobarbital (40 mg/kg), and then a cannula (PE8050, Natsume, Tokyo, Japan) was inserted into the arteria femoralis before PFD was administered orally. Blood samples (approximately 150 μL) were collected from the cannulated arteria femoralis at the indicated times (0.083, 0.25, 0.5, 0.75, 1, 1.5, 2, 3, 4, and 6 h) after oral administration of PFD (30 and 160 mg/kg). Plasma obtained by centrifugation (10000g, 10 min, 4 °C) was deproteinized by the addition of ACN. The mixture was mixed for a few seconds and centrifuged (2000 rpm, 1 min, 4 °C). The supernatants were filtered and diluted with 50% ACN solution. Then, 50% ACN solution including antipyrine (5 μg/mL), an internal standard, was added to them (diluted supernatant:antipyrine = 9:1) for UPLC analysis.

2.11. Tissue deposition of PFD after oral administration

At the indicated times (0.083, 0.5, 1, 2, 3, 4, and 6 h) after oral administration of PFD (30 and 160 mg/kg), rats were sacrificed by taking blood from the descending aorta under temporary anesthesia with diethyl ether, and the tissues were then perfused with cold saline from the aorta. The skin, lung, and eyes were dissected, and then fat and blood vessels were removed by trimming. The tissues were minced with scissors in stoppered test tubes and homogenized using a Physcotron (Microtech, Chiba, Japan) in 4 mL of ACN. After shaking for 5 min and sonication for 10 min, the mixtures were centrifuged (3000 rpm, 10 min). Extraction was repeated two times with ACN and the supernatants were pooled. The samples were evaporated to dryness under a gentle stream of nitrogen at 45 °C. The residues were dissolved in 50% ACN solution containing antipyrine (500 ng/mL) as an internal standard for UPLC analysis.

2.12. UPLC analysis

The concentrations of PFD in rat tissues and plasma were determined by ultra performance liquid chromatography equipped with electrospray ionization mass spectrometry (UPLC/ESI-MS) analysis. The UPLC/ESI-MS system consisted of a Waters Acquity UPLC™ system (Waters, Milford, MA, USA), which included a binary solvent manager, a sample manager, a column compartment, and a Micromass SQ detector connected with Waters Masslynx v 4.1. A Waters Acquity UPLC™ BEH C_{18} (particle size: 1.7 μm, column size: ϕ2.1 × 50 mm; Waters) was used, and column temperature was maintained at 40 °C. The standards and samples were separated using a gradient mobile phase consisting of Milli-Q containing 5 mM ammonium acetate (A) and methanol (B). The gradient condition of the mobile phase was 0–0.5 min, 75% A; 0.5–4 min, 75–40% A; 4–5 min, 5% A; 5–6 min, 75% A, and the flow rate was set at 0.25 mL/min. Analysis was carried out using SIR for specific m/z: 186 $[M+1]^+$ for PFD; and 189 $[M+1]^+$ for antipyrine (internal standard).

2.13. Pharmacokinetic analysis

Pharmacokinetic characterization in the plasma was performed by non-compartmental analysis as implemented in WinNonlin Professional Version 5.2 (Pharsight Corporation, Mountain View, CA, USA) and that in skin was carried out by non-compartmental analysis. The elimination rate constant (k_{el}) was estimated by the least square method from the terminal phase. The elimination half-life ($t_{1/2}$) was calculated using the following equation:

$$t_{1/2} = \frac{\ln 2}{k_{el}}$$

Area under concentration *versus* time curve ($AUC_{0\to\infty}$), area under moment curve ($AUMC_{0\to\infty}$), and mean residence time (MRT) were estimated using a trapezoid formula from 0 h to the last measurement time (T), after which the last observed concentration (C_T) and $t_{1/2}$ were used as follows:

$$AUC_{0\to\infty} = \int_0^T C dt + \frac{C_T}{k_{el}}$$

$$AUMC_{0\to\infty} = \int_0^T t \cdot C dt + \frac{T \cdot C_T}{k_{el}} + \frac{C_T}{k_{el}^2}$$

$$MRT = \frac{AUMC_{0\to\infty}}{AUC_{0\to\infty}}$$

where C is the observed plasma or skin concentration (plasma: ng/mL, skin: ng/g skin) and t equals the measurement time (h).

2.14. Data analysis

For statistical comparisons, one-way analysis of variance (ANOVA) with pairwise comparison by Fisher's least significant difference procedure was used. A P value of less than 0.05 was considered significant for all analyses.

Standard error of each PK parameter in tissues was defined by the delta method using the root of the following equation [20,21]:

$$V(\overline{AUC}_{0\to\infty}) = \sum_{i=2}^{m}[(V(C_i)/n_i + V(C_{i-1})/n_{i-1}) \times ((t_i - t_{i-1})/2)^2] + (1/k_{el})^2 \cdot V(C_T)/n_T + (C_T/k_{el})^2 \cdot V(k_{el})/n_\lambda$$

$$V(\overline{AUMC}_{0\to\infty}) = \sum_{i=2}^{m}[(V(C_i)/n_i + V(C_{i-1})/n_{i-1}) \times ((t_i - t_{i-1})/2)^2] + (1/k_{el}^2)^2 \cdot V(C_T)/n_T + (C_T \cdot 2/k_{el}^3)^2 \cdot V(k_{el})/n_\lambda + (1/k_{el})^2 \cdot V(C_T)/n_T + (T \cdot C_T/k_{el}^2)^2 \cdot V(k_{el})/n_\lambda$$

$$V(\overline{MRT}) = \frac{V(\overline{AUMC}_{0\to\infty})}{(AUC_{0\to\infty})^2} + \frac{V(\overline{AUC}_{0\to\infty}) \cdot (AUMC_{0\to\infty})^2}{(AUC_{0\to\infty})^4}$$

where m is the number of collection points, C_i is equal to the skin concentration of PFD, t_i equals the collection time, and n_i represents the number of each collection time.

3. Results and discussion

3.1. Photochemical properties of PFD

As a primary event of phototoxic reactions, photosensitizers are excited by the absorption of photon energy from sunlight, and then the photoexcited chemicals can react with other molecules via energy transfer and/or radical reactions, possibly leading to phototoxic reactions. To estimate the photoexcitability of compounds, a UV spectral analysis is recommended by European and American guidelines for photosafety testing. The UV spectral pattern of PFD was recorded in 20 mM NaPB (pH 7.4; Fig. 2). According to the UV spectral pattern of PFD, intense UV absorption of PFD was observed in the UVA/B region, partly overlapping with the sunlight spectrum [22]. The lowest energy band in the UVA/B region had a maximum at ca. 313 nm, and the molar extinction coefficient (MEC) of PFD was calculated to be ca. 6450 M^{-1} cm^{-1}. On the basis of the results from the UV spectral analysis, PFD could be excited by sunlight, and potentially cause photochemical reactions, possibly leading to phototoxic skin responses. The Organisation for Economic Co-operation and Development (OECD) guidelines have stated the criterion of a MEC at 10 M^{-1} cm^{-1} for deciding whether photosafety evaluation on chemicals is needed [23]. Additionally, Henry et al. proposed that photosafety testing on chemicals might not be needed if the MEC of a compound is estimated to be less than 1000 M^{-1} cm^{-1} in UV absorption spectral analysis [24]. Considering the guidelines and previous reports, further photosafety evaluations on PFD were needed to characterize its phototoxic risk.

ROS, including singlet oxygen and superoxide, are well known as principal toxic mediators in early phototoxic events. Singlet oxygen and superoxide were generated from photoirradiated chemicals via type II and I photochemical reactions, respectively, and the ROS are responsible for oxidative damage against biomolecules [1], possibly leading to phototoxic reactions. On the basis of the phototoxic pathways, the phototoxic potential of compounds could be elucidated by monitoring ROS generation from compounds under exposure to UV radiation. To evaluate the phototoxic potential of PFD, the ROS assay on PFD, KPF and ETM was carried out (Fig. 3). KPF has been identified as phototoxic and photogenotoxic [25], mechanism of which is thought to be ROS generation [26]. ETM was characterized as a non/weak phototoxic chemical in ROS assay and a 3T3 neutral red uptake phototoxicity testing [27]. Therefore, in the present study, KPF and ETM were used as positive and negative controls, respectively. Photoirradiated PFD at 20 μM or much higher concentrations yielded singlet oxygen in a concentration-dependent manner (Fig. 3A), and photoirradiated PFD at concentrations of more than 100 μM exhibited concentration-dependent generation of superoxide (Fig. 3B). Onoue and coworkers previously proposed tentative criteria on the ROS assay to discriminate the photosensitizers from non-phototoxic substances on the basis of ROS data on marketed drugs at concentration of 200 μM [28], and the criteria were set at 2.0×10^{-2} for singlet oxygen and 2.5×10^{-2} for superoxide. KPF (200 μM) also generated both singlet oxygen and superoxide under exposure to simulated sunlight, and ROS generation from ETM (200 μM), in contrast, could not be detected in the present conditions. According to the results from the ROS assay, like a KPF [26], PFD would have high photoreactivity and would potentially cause phototoxic reactions via both type I and type II photochemical reactions upon exposure to sunlight.

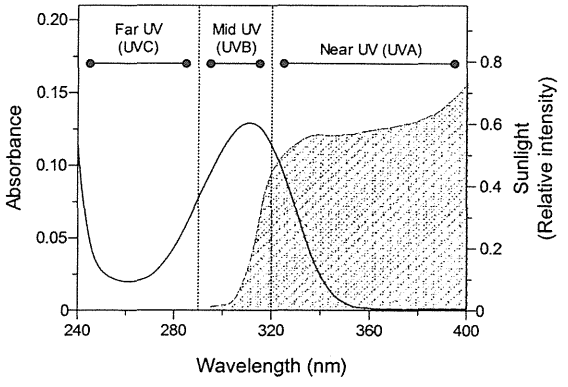

Fig. 2. UV absorption spectra of PFD in 20 mM NaPB (pH 7.4) and average intensity of sunlight at the earth's surface. Solid line: PFD. Average intensity of sunlight (shaded) was reproduced from a previous report [22].

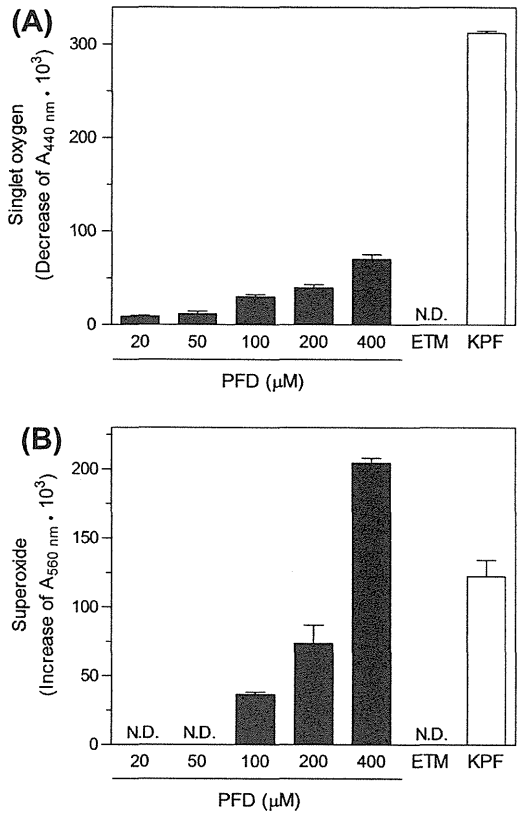

Fig. 3. Generation of reactive oxygen species from PFD exposed to simulated sunlight. (A) Singlet oxygen and (B) superoxide. Data represent mean ± SD of three experiments.

3.2. Characterization of in vitro phototoxicity of PFD

On the basis of the photochemical assessments, PFD was deduced to have phototoxic risk, the detailed mechanisms of which have not been fully elucidated. Herein, *in vitro* photoirritancy of PFD was assessed using the generation of TBARS, and the IBP assay and the AGE-based photogenotoxicity test were conducted to evaluate the *in vitro* photogenotoxicity of PFD.

A previous study demonstrated that several phototoxic drugs accelerated the peroxidation of linoleic acid upon exposure to simulated sunlight [4], and the photodynamic lipid peroxidation in the cellular membrane has been considered to be one of the major mechanisms in the drug-induced photoirritation [29]. In

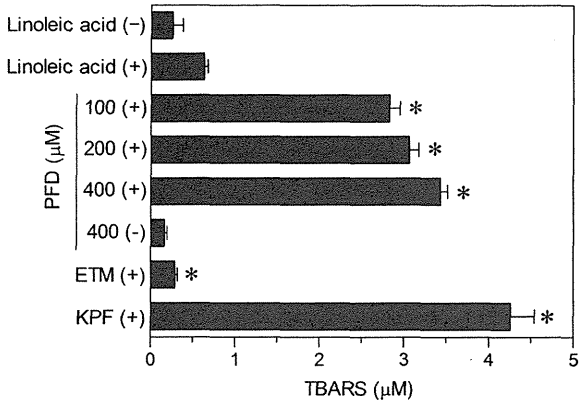

Fig. 4. Lipid peroxidation induced by irradiated compounds. Linoleic acid (+) or (−) indicates the linoleic acid with or without UVA/B irradiation, respectively. Data represent mean ± SD of 3 determinations. *$P < 0.05$ with respect to linoleic acid (+).

our previous study, ROS scavengers could attenuate phototoxin-induced peroxidation of fatty acid under exposure to simulated sunlight, and these findings suggested involvement of ROS generation in the photodynamic lipid peroxidation by phototoxins [30,31]. Thus, photosensitized peroxidation of linoleic acid by PFD was monitored to evaluate its photoirritant risk (Fig. 4). UV irradiation of linoleic acid (1 mM) without chemicals yielded a small amount of peroxidation products; however, irradiation with KPF (200 μM) produced a much greater amount of TBARS, and irradiated PFD at the indicated concentrations also exhibited significant generation of lipoperoxidants in a concentration-dependent manner. In contrast, the addition of ETM (200 μM) did not show any significant lipid peroxidation under the present experimental conditions, and PFD (400 μM) kept in the dark did not lead to enhanced lipid peroxidation. On the basis of the ability for photodynamic lipid peroxidation, PFD would have a potent *in vitro* photoirritancy.

Some photosensitizers induce DNA impairment under exposure to UVA/B, such as formation of photoadducts, pyrimidine dimers, and oxidative DNA modifications [32]. Thus, the DNA impairment of PFD was monitored using the IBP assay (Fig. 5A). The IBP assay can evaluate the photodynamic impairment of dsDNA by chemicals based on the differences of fluorescence emission from DNA-intercalator complexes between control and irradiated groups [33]. Since the significant decrease of intercalated TO levels was observed between the control and irradiated groups of KPF (200 μM), KPF would have a potent phototoxic risk. In contrast, there were no significant decreases of intercalated TO levels between the control and irradiated groups of PFD at any irradiated concentrations, and thus, photodynamic DNA impairment by PFD was not too strong. To confirm the photogenotoxic potential of PFD deduced from the IBP data, the structure conversion of plasmid pBR322 DNA by phototoxins was also monitored by AGE analysis (Fig. 5B). According to the AGE analysis, irradiated KPF (200 μM) led to marked damage of pBR322 DNA; however, photodynamic DNA impairment by ETM (200 μM) and PFD at the indicated concentrations was not observed. The DNA-photocleaving data on tested chemicals from AGE analysis were consistent with the results from the IBP assay, and the photogenotoxic potential of PFD was negligible.

Photosensitive skin rash was frequently observed in the phase II and III clinical trials on PFD, and some patients discontinued taking PFD due to the photosensitive skin rash [11,14,16]. Raghu et al. also reported that the photosensitive reaction was settled by aborting administration of PFD in all cases [14]. Thus, the present *in vitro* observations on PFD would be in agreement with the photosafety data in clinical use.

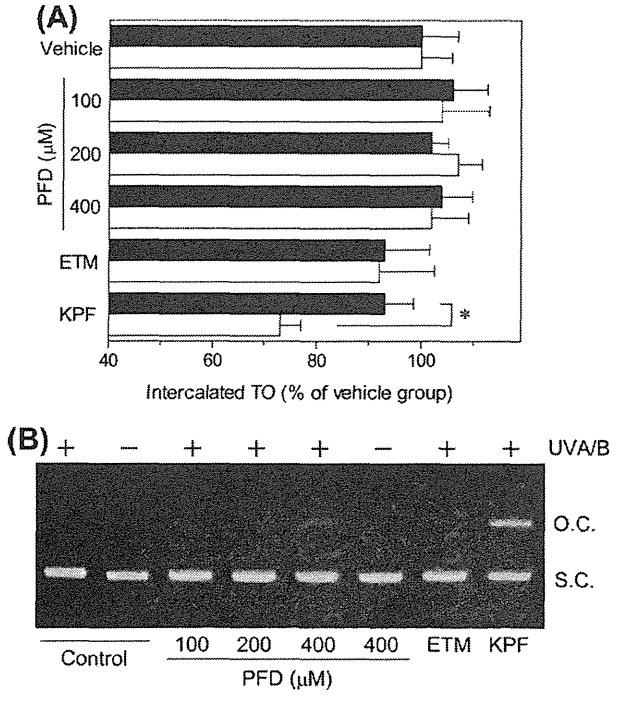

Fig. 5. Photogenotoxic potential of compounds. (A) DNA damage induced by photoirradiated compounds. Open bar, UV irradiated; and filled bar, control group. Data represent mean ± SD of four experiments. *$P < 0.05$ between indicated groups. (B) DNA-photocleavage assay for predicting photogenotoxic potential. OC, open circular form; and SC, supercoiled form. According to AGE analysis, the photodynamic impairment of pBR322 DNA is expressed as % of OC form.

3.3. Colorimetrical evaluation of cutaneous changes

Photoirritant potential of PFD was found by monitoring the photosensitized peroxidation of linoleic acid, and the finding would have some relationship to previous clinical observations. However, it was still unclear if PFD could cause photoirritant skin responses *in vivo*. Therefore, *in vivo* cutaneous inflammation in rats, possibly caused by orally administered PFD and UV irradiation, was examined using a colorimeter, in which the differences in color (ΔE) between before and after treatment were estimated on the basis of L^*, a^*, and b^* values. From the previous investigations, PFD could be detected in rat plasma around 15 min after oral administration [34], and PFD (100 mg/kg/day, t.i.d.) significantly suppressed bleomycin-induced pulmonary fibrosis in mice [35]. In the preliminary examination for the *in vivo* phototoxicity test, colorimetrical change on the surface of rat skin was perceptible after oral administration of PFD (160 mg/kg), followed by exposure to UVA light. On the basis of the previous reports and the preliminary examination, the present *in vivo* phototoxicity testing on PFD was designed, and the obtained results were described in Table 1. In the colorimetrical evaluation on the surface of the skin, the ΔE values of non-irradiated rats treated with PFD (30 and 160 mg/kg, p.o.) were not significantly different from those of non-irradiated rats in the vehicle group. The ΔE values of UV-exposed rats in all groups were higher than those of non-irradiated rats in corresponding groups, and the difference in ΔE values between UV-exposed and non-exposed rats could be attributable to the increase of a^* and b^* values in UV-exposed group as observed in previous study [36]. Orally administered PFD (30 mg/kg) led to no significant colorimetrical changes on

Table 1
Colorimetrical evaluation of skin inflammation.

	UV		Colorimetrical evaluation			
			L^*	a^*	b^*	ΔE
Vehicle	–	Initial	64.91	1.26	7.19	1.13 ± 0.34
		Treated	65.98	1.03	7.07	
	+	Initial	71.22	1.30	2.29	2.26 ± 0.19
		Treated	69.23	1.92	3.03	
PFD (30 mg/kg)	–	Initial	70.16	1.19	−0.18	1.47 ± 0.27
		Treated	71.56	1.54	−0.36	
	+	Initial	72.90	1.27	4.14	2.40 ± 0.20
		Treated	72.26	2.81	5.72	
PFD (160 mg/kg)	–	Initial	70.59	0.09	3.67	1.69 ± 0.24
		Treated	71.04	−1.04	4.88	
	+	Initial	71.05	0.89	5.67	3.97 ± 0.59
		Treated	72.35	2.06	9.17	

Cutaneous inflammation after oral administration of PFD with or without UV exposure was evaluated using a colorimeter with the $L^*a^*b^*$ system. The differences in color (ΔE) between before and after treatment were estimated on the basis of L^*, a^*, and b^* values. Each L^*, a^*, and b^* value represents mean and each ΔE value represents mean ± SD for three determinations.

the surface of the skin after exposure to UV compared with the ΔE value of UV-exposed vehicle group. In contrast, UV-exposed rats with orally administered PFD (160 mg/kg) indicated significantly higher ΔE values than the UV-exposed rats in other groups in the present evaluation ($P < 0.05$) due to the increase of b^* value (Δb^*: 3.5). In our previous study, photoirradiated griseofulvin, a typical phototoxic drug, also caused the increase of b^* value (Δb^*: 4.3) in rats [6]. Thus, the present results would indicate the photoirritant skin responses by orally administered PFD (160 mg/kg). PFD-induced phototoxicity, especially photoirritant skin responses, seemed to depend on the dosage of PFD in the present single dosing regimen. Non-phototoxic (30 mg/kg) and phototoxic (160 mg/kg) doses of PFD could tentatively be deduced on the basis of the results from *in vivo* phototoxicity test. In the previous clinical trial [16], dose-dependent phototoxicity was not found because the frequency of PFD-induced phototoxicity was 52.7% in the low-dose group (1.2 g/day of PFD) and 51.4% in the high-dose group (1.8 g/day). The discrepancy between the previous clinical trial and our *in vivo* phototoxicity test might be attributable to uncontrolled UV irradiation in the previous clinical trial and/or the differences of PFD dosage between low and high doses (1.5-fold in the clinical trial and ca. 5-fold in the *in vivo* phototoxicity test).

3.4. Pharmacokinetic assessments of PFD after oral administration

On the basis of the results from *in vivo* phototoxic test, tentative phototoxic and non-phototoxic doses could be determined; however, the effects of systemic exposure of PFD and its distribution to UV-exposed tissues after oral administration are still unclear. In particular, estimated PK parameters for compounds in the skin are important as crucial factors for the photosafety assessment strategies. Phototoxic chemicals initially distribute to the skin, and, then, the phototoxic chemicals can be excited by UVA/B radiation [6,7]. Therefore, the PK behaviors on PFD were characterized after oral administration. The concentration–time curves of PFD in the plasma, skin, eyes, and lungs were obtained by UPLC-ESI/MS analysis after oral administration of PFD (30 and 160 mg/kg;

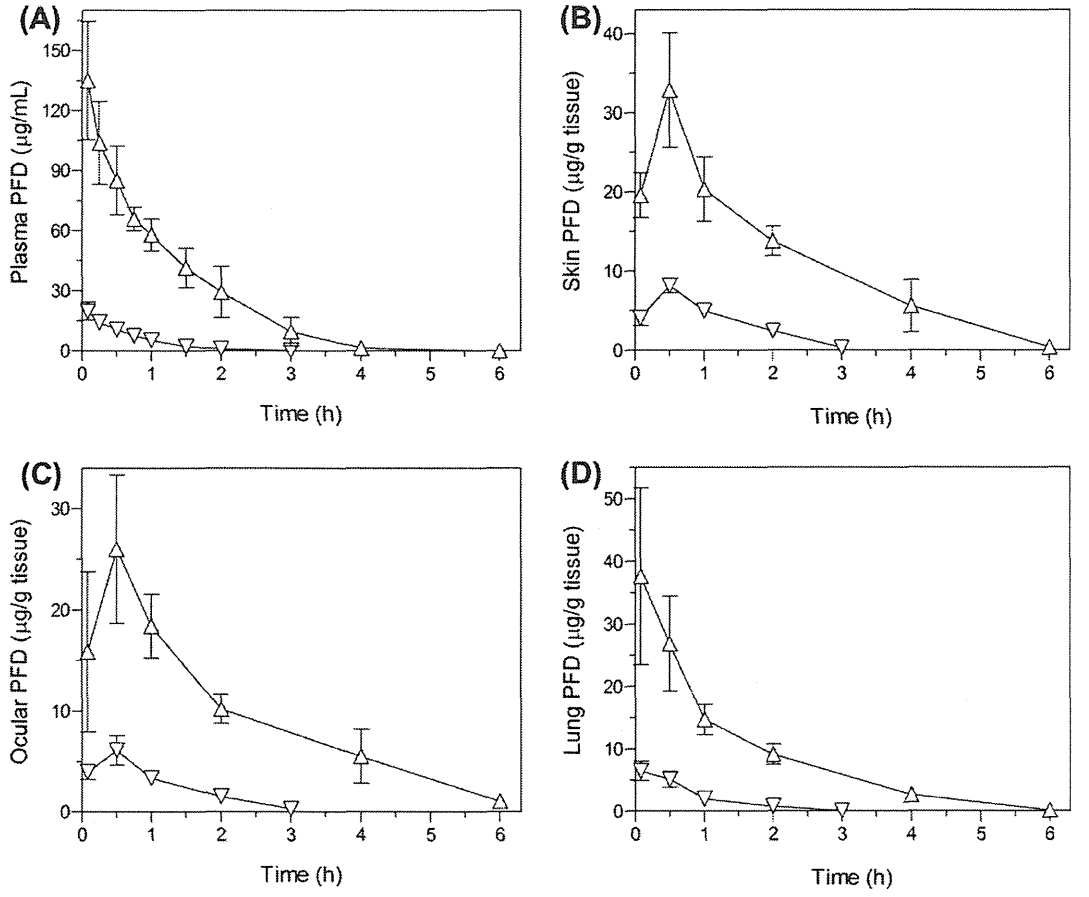

Fig. 6. Concentration–time profiles of PFD in plasma (A), skin (B), eyes (C) and lungs (D) after oral administration of PFD in rats. ▽, PFD at a phototoxic dose (30 mg/kg); and △, PFD at a non-phototoxic dose (160 mg/kg). Each value represents mean ± SD for 4–8 rats.

Table 2
PK parameters of PFD after oral administration in rats.

	C_{max} (plasma, μg/mL; tissues, μg/g tissue)	$t_{1/2}$ (h)	$AUC_{0\to\infty}$ (plasma, h·μg/mL; tissues, h·μg/g tissue)	MRT (h)
PFD (30 mg/kg, p.o.)				
Plasma	19.7 ± 1.9	0.33 ± 0.03	14.1 ± 1.8	0.67 ± 0.19
Skin	8.2 ± 1.0	1.07 ± 0.56	11.5 ± 1.0	1.14 ± 0.23
Eyes	4.0 ± 0.6	0.67 ± 0.35	8.3 ± 0.8	1.06 ± 0.25
Lung	6.5 ± 1.3	0.80 ± 0.47	6.5 ± 0.8	0.79 ± 0.31
PFD (160 mg/kg, p.o.)				
Plasma	135.0 ± 22.0	0.53 ± 0.07	152.0 ± 20.0	1.05 ± 0.15
Skin	32.9 ± 5.1	1.06 ± 0.47	68.0 ± 2.7	1.70 ± 0.09
Eyes	26.0 ± 5.1	1.06 ± 0.53	58.8 ± 2.5	1.93 ± 0.10
Lung	37.6 ± 11.1	0.77 ± 0.31	52.1 ± 2.0	1.32 ± 0.08

Each value represents mean ± SD for 4–8 rats.

Fig. 6). On the basis of the data obtained, the relevant PK parameters of PFD were also estimated including maximum concentration (C_{max}), $t_{1/2}$, $AUC_{0\to\infty}$, and MRT, and the calculated PK parameters are summarized in Table 2. After oral administration of PFD (30 and 160 mg/kg), the plasma and lung concentrations immediately reached the C_{max} at 5 min, and subsequently the C_{max} of PFD in the skin and eyes, in which phototoxic responses would occur, were observed at 30 min after oral administration. Thus, orally administered PFD could potentially cause phototoxic skin responses around 30 min in the present dosing regimens. In both low and high dose groups, the calculated C_{max} values in the plasma and tissues were quite different. Compared with PFD at low dose (30 mg/kg), oral administration of PFD at high dose (160 mg/kg) led to significant increases of C_{max} values in the plasma and tissues by 4–7-fold. The $AUC_{0\to\infty}$ values in the plasma and tissues after oral administration of PFD (160 mg/kg) were from 6-fold to 11-fold higher than those after oral administration of PFD (30 mg/kg). According to the $t_{1/2}$ and MRT values, orally administered PFD (160 mg/kg) had longer-term exposure risk compared with orally administered PFD (30 mg/kg). Compared with the PK parameters in the lungs, PFD tended to exhibit exposure in the skin and eyes and retention in the skin and eyes for the higher PK parameters.

In our previous investigation, the *in vivo* phototoxic risk of fluoroquinolones was evaluated by *in vitro* phototoxic assessments and *in vivo* PK analysis [7]. Norfloxacin and ciprofloxacin exhibited potent *in vitro* phototoxicity; however, they were evaluated to have less *in vivo* phototoxic potential due to their lower skin distribution properties. Thus, lower skin distribution of phototoxic chemicals would lead to less phototoxic responses in the skin. The differences of skin exposure to PFD were observed between phototoxic (160 mg/kg) and non-phototoxic (30 mg/kg) doses on the basis of the PK profiles, and the skin distribution properties might, to some extent, be related to the observation on the *in vivo* phototoxicity test. Therefore, controlling the skin exposure to PFD and/or UV might be of great benefit to avoid or reduce the phototoxic potential of PFD. Indeed, patients taking PFD are usually advised to avoid exposure to sunlight by using photoprotective clothing and sunscreens. For a benefit of the patients, marked reduction of PFD dosage in oral administration would be useful for attenuating PFD-induced phototoxicity, although it might be a risk for offset of its pharmacological effects. Strategic development of well-suited drug delivery systems for lung targeting might be efficacious for controlling phototoxic risk of PFD without attenuating its pharmacological effects. For clinical treatment of idiopathic pulmonary fibrosis, PFD has to be taken three times a day, and accumulated metabolites of PFD might cause phototoxic skin responses. Further photosafety studies on metabolites of PFD would be needed for better understanding of phototoxicity of PFD.

4. Conclusion

PFD was found to be photoreactive, and the generation of ROS from UV-exposed PFD might lead to a photoirritation risk, but not to photogenotoxic potential. Orally administered PFD at a dose of 160 mg/kg was phototoxic in rats, whereas the phototoxic skin responses were negligible for PFD at a lower dose (30 mg/kg). After oral administration of PFD, the distribution of PFD to the UV-exposed tissues such as skin and eyes was higher than that in the lungs. From these findings, a high dose of PFD might cause phototoxic responses through the generation of ROS in the skin, and strategic application of appropriate drug delivery systems might be efficacious for reducing phototoxic risk by modulation of skin exposure to the PFD.

5. Abbreviations

ACN	acetonitrile
AGE	agarose gel electrophoresis
ANOVA	analysis of variance
$AUC_{0\to\infty}$	area under concentration *versus* time curve
$AUMC_{0\to\infty}$	area under moment curve
BHT	butylated hydroxytoluene
CIE	Commission Internationale de l'Eclairage
C_{max}	maximum concentration
EtBr	ethidium bromide
ETM	erythromycin
IBP	Intercalator-based photogenotoxicity
k_{el}	elimination rate constant
KPF	ketoprofen
MEC	molar extinction coefficient
MRT	mean residence time
NaPB	sodium phosphate buffer
NBT	nitroblue tetrazolium
OECD	Organisation for Economic Co-operation and Development
PFD	pirfenidone
PK	pharmacokinetic
RNO	*p*-nitrosodimethylaniline
ROS	reactive oxygen species
$t_{1/2}$	elimination half-life
TAE	Tris–acetate-EDTA
TBA	thiobarbituric acid
TBARS	TBA-reactive substances
TO	thiazole orange
UPLC/ESI-MS	ultra performance liquid chromatography equipped with electrospray ionization mass spectrometry
UV	ultraviolet

Acknowledgement

Authors are grateful to Shionogi & Co., Ltd. for kindly providing pirfenidone. This work was supported in part by a Health Labour Sciences Research Grant from The Ministry of Health, Labour and Welfare, Japan.

References

[1] J.H. Epstein, Phototoxicity and photoallergy in man, J. Am. Acad. Dermatol. 8 (1983) 141–147.

[2] J.H. Epstein, B.U. Wintroub, Photosensitivity due to drugs, Drugs 30 (1985) 42–57.
[3] H. Spielmann, M. Liebsch, B. Doring, F. Moldenhauer, First results of an EC/COLIPA validation project of *in vitro* phototoxicity testing methods, Altex 11 (1994) 22–31.
[4] S. Onoue, Y. Tsuda, Analytical studies on the prediction of photosensitive/phototoxic potential of pharmaceutical substances, Pharmaceut. Res. 23 (2006) 156–164.
[5] S. Onoue, K. Kawamura, N. Igarashi, Y. Zhou, M. Fujikawa, H. Yamada, Y. Tsuda, Y. Seto, S. Yamada, Reactive oxygen species assay-based risk assessment of drug-induced phototoxicity: classification criteria and application to drug candidates, J. Pharm. Biomed. Anal. 47 (2008) 967–972.
[6] Y. Seto, S. Onoue, S. Yamada, *In vitro/in vivo* phototoxic risk assessments of griseofulvin based on photobiochemical and pharmacokinetic behaviors, Eur. J. Pharm. Sci. 38 (2009) 104–111.
[7] Y. Seto, R. Inoue, M. Ochi, G. Gandy, S. Yamada, S. Onoue, Combined use of in vitro phototoxic assessments and cassette dosing pharmacokinetic study for phototoxicity characterization of fluoroquinolones, AAPS J. 13 (2011) 482–492.
[8] J. Macias-Barragan, A. Sandoval-Rodriguez, J. Navarro-Partida, J. Armendariz-Borunda, The multifaceted role of pirfenidone and its novel targets, Fibrogenesis Tissue Repair 3 (2010) 16.
[9] S. Mirkovic, A.M. Seymour, A. Fenning, A. Strachan, S.B. Margolin, S.M. Taylor, L. Brown, Attenuation of cardiac fibrosis by pirfenidone and amiloride in DOCA-salt hypertensive rats, Brit. J. Pharmacol. 135 (2002) 961–968.
[10] F.S. Shihab, W.M. Bennett, H. Yi, T.F. Andoh, Pirfenidone treatment decreases transforming growth factor-beta1 and matrix proteins and ameliorates fibrosis in chronic cyclosporine nephrotoxicity, Am. J. Transplant.: Off. J. Am. Soc. Transplant. Am. Soc. Transplant Surgeons 2 (2002) 111–119.
[11] L. Garcia, I. Hernandez, A. Sandoval, A. Salazar, J. Garcia, J. Vera, G. Grijalva, P. Muriel, S. Margolin, J. Armendariz-Borunda, Pirfenidone effectively reverses experimental liver fibrosis, J. Hepatol. 37 (2002) 797–805.
[12] J.P. Kehrer, S.B. Margolin, Pirfenidone diminishes cyclophosphamide-induced lung fibrosis in mice, Toxicol. Lett. 90 (1997) 125–132.
[13] T.M. Maher, Pirfenidone in idiopathic pulmonary fibrosis, Drugs Today (Barc) 46 (2010) 473–482.
[14] G. Raghu, W.C. Johnson, D. Lockhart, Y. Mageto, Treatment of idiopathic pulmonary fibrosis with a new antifibrotic agent, pirfenidone: results of a prospective, open-label Phase II study, Am. J. Respir. Crit. Care Med. 159 (1999) 1061–1069.
[15] P.W. Noble, C. Albera, W.Z. Bradford, U. Costabel, M.K. Glassberg, D. Kardatzke, T.E. King Jr., L. Lancaster, S.A. Sahn, J. Szwarcberg, D. Valeyre, R.M. du Bois, Pirfenidone in patients with idiopathic pulmonary fibrosis (CAPACITY): two randomised trials, Lancet 377 (2011) 1760–1769.
[16] H. Taniguchi, M. Ebina, Y. Kondoh, T. Ogura, A. Azuma, M. Suga, Y. Taguchi, H. Takahashi, K. Nakata, A. Sato, M. Takeuchi, G. Raghu, S. Kudoh, T. Nukiwa, Pirfenidone in idiopathic pulmonary fibrosis, Eur. Respir. J. 35 (2010) 821–829.
[17] H. Ohkawa, N. Ohishi, K. Yagi, Assay for lipid peroxides in animal tissues by thiobarbituric acid reaction, Anal. Biochem. 95 (1979) 351–358.
[18] G.E. Pierard, C. Pierard-Franchimont, Dihydroxyacetone test as a substitute for the dansyl chloride test, Dermatology 186 (1993) 133–137.
[19] W. Westerhof, B.A. van Hasselt, A. Kammeijer, Quantification of UV-induced erythema with a portable computer controlled chromameter, Photodermatology 3 (1986) 310–314.
[20] S. Takemoto, K. Yamaoka, M. Nishikawa, Y. Takakura, Histogram analysis of pharmacokinetic parameters by bootstrap resampling from one-point sampling data in animal experiments, Drug Metab. Pharmacokinet. 21 (2006) 458–464.
[21] A.J. Bailer, Testing for the equality of area under the curves when using destructive measurement techniques, J. Pharmacokinet. Biopharm. 16 (1988) 303–309.
[22] J. Jagger, Solar-UV Actions on Living Cells, Praeger Scientific, New York, 1985.
[23] OECD, OECD guideline for testing of chemicals, 432, In vitro 3T3 NRU phototoxicity test, The Organisation for Economic Co-operation and Development, 2004.
[24] B. Henry, C. Foti, K. Alsante, Can light absorption and photostability data be used to assess the photosafety risks in patients for a new drug molecule?, J Photochem. Photobiol. B 96 (2009) 57–62.
[25] T. Nakazawa, T. Shimo, N. Chikamatsu, T. Igarashi, O. Nagata, M. Yamamoto, Study on the mechanism of photosensitive dermatitis caused by ketoprofen in the guinea pig, Arch. Toxicol. 80 (2006) 442–448.
[26] S. Liu, H. Mizu, H. Yamauchi, Photoinflammatory responses to UV-irradiated ketoprofen mediated by the induction of ROS generation, enhancement of cyclooxygenase-2 expression, and regulation of multiple signaling pathways, Free Radical Biol. Med. 48 (2010) 772–780.
[27] S. Onoue, M. Ochi, G. Gandy, Y. Seto, N. Igarashi, Y. Yamauchi, S. Yamada, High-throughput screening system for identifying phototoxic potential of drug candidates based on derivatives of reactive oxygen metabolites, Pharmaceut. Res. 27 (2010) 1610–1619.
[28] S. Onoue, N. Igarashi, S. Yamada, Y. Tsuda, High-throughput reactive oxygen species (ROS) assay: an enabling technology for screening the phototoxic potential of pharmaceutical substances, J. Pharm. Biomed. Anal. 46 (2008) 187–193.
[29] J.V. Castell, M.J. Gomez-Lechon, C. Grassa, L.A. Martinez, M.A. Miranda, P. Tarrega, Photodynamic lipid peroxidation by the photosensitizing nonsteroidal antiinflammatory drugs suprofen and tiaprofenic acid, Photochem. Photobiol. 59 (1994) 35–39.
[30] S. Onoue, N. Igarashi, Y. Yamauchi, T. Kojima, N. Murase, Y. Zhou, S. Yamada, Y. Tsuda, In vitro phototoxic potential and photochemical properties of imidazopyridine derivative: a novel 5-HT4 partial agonist, J. Pharm. Sci. 97 (2008) 4307–4318.
[31] S. Onoue, N. Igarashi, Y. Yamauchi, N. Murase, Y. Zhou, T. Kojima, S. Yamada, Y. Tsuda, In vitro phototoxicity of dihydropyridine derivatives: a photochemical and photobiological study, Eur. J. Pharm. Sci. 33 (2008) 262–270.
[32] S. Brendler-Schwaab, A. Czich, B. Epe, E. Gocke, B. Kaina, L. Muller, D. Pollet, D. Utesch, Photochemical genotoxicity: principles and test methods, Report of a GUM Task Force, Mutation Research 566 (2004) 65–91.
[33] Y. Seto, M. Ochi, S. Onoue, S. Yamada, High-throughput screening strategy for photogenotoxic potential of pharmaceutical substances using fluorescent intercalating dye, J. Pharm. Biomed. Anal. 52 (2010) 781–786.
[34] Y. Wang, X. Zhao, J. Zhong, Y. Chen, X. Liu, G. Wang, Simple determination of pirfenidone in rat plasma via high-performance liquid chromatography, Biomed. Chromatogr.: BMC 20 (2006) 1375–1379.
[35] H. Oku, T. Shimizu, T. Kawabata, M. Nagira, I. Hikita, A. Ueyama, S. Matsushima, M. Torii, A. Arimura, Antifibrotic action of pirfenidone and prednisolone: different effects on pulmonary cytokines and growth factors in bleomycin-induced murine pulmonary fibrosis, Eur. J. Pharmacol. 590 (2008) 400–408.
[36] T. Nose, K. Tsurumi, Pharmacological studies on cutaneous inflammation induced by ultraviolet irradiation (1): quantification of erythema by reflectance colorimetry and correlation with cutaneous blood flow, Jpn. J. Pharmacol. 62 (1993) 245–256.

Research Article

Journal of Applied Toxicology

Received: 24 August 2012, Revised: 27 September 2012, Accepted: 31 October 2012 Published online in Wiley Online Library

(wileyonlinelibrary.com) DOI 10.1002/jat.2846

Development of an albuminous reactive oxygen species assay for photosafety evaluation under experimental biomimetic conditions

Satomi Onoue*, Masashi Kato and Shizuo Yamada

ABSTRACT: The generation of reactive oxygen species (ROS) from an ultraviolet (UV)-exposed chemical can be an experimental indicator of phototoxic potential. The aim of the present study was to develop a new ROS assay using serum albumin to provide photosafety assessment under experimental biomimetic conditions. To assess assay robustness, a validation study on an albuminous ROS (aROS) assay was conducted with a focus on intra- and inter-day precisions and Z′-factor reflecting both the assay signal-to-noise ratio and variation associated with signal measurements. In the aROS assay on quinine HCl (200 μM), a typical phototoxic drug, both intra- and inter-day precisions (coefficient of variation; CV) were found to be below 4%, and the Z′-factors for singlet oxygen and superoxide suggested a large separation band between samples and blank signals. To evaluate the prediction capacity, the aROS and ROS assays were applied to 21 phototoxins and 10 non-phototoxic chemicals. Upon aROS assay on these model chemicals, the individual specificity was 100%, and the positive and negative predictivities were found to be 100% and 81.8%, respectively. The aROS assay can be employed for poorly soluble chemicals for which the ROS assay is unavailable. Comparing the ROS assay data, there seemed to be a photochemical transition of some chemicals in albuminous solution. A molecular interaction between albumin and chemical was also assessed by UV and fluorescent spectroscopic analyses, and the results suggested the limited relationship between the albumin–chemical interaction and the photochemical change. The aROS assay may allow photosafety assessment of new drug entities with a wide range of applicability partly under experimental biomimetic conditions. Copyright © 2013 John Wiley & Sons, Ltd.

Keywords: albumin; photoreactivity; photosafety assessment; phototoxicity; reactive oxygen species

Introduction

Phototoxic skin responses can be caused by the combined effects of external phototoxic drugs and sunlight irradiation, consisting of partial ultraviolet (UV) B, UVA and visible (VIS) lights (Stein and Scheinfeld, 2007); the side effects could lead to reductions in medication compliance. There are at least three types of phototoxic reaction, including photoirritation, photogenotoxicity and photoallergy, with different mechanisms and pathologic features (Moore, 2002). To date, in order to avoid these drug-induced phototoxic reactions, considerable efforts have been made, which include the clinical use of a sunscreen (Dubakiene and Kupriene, 2006), the development of a new formulation for controlling the skin distribution of drugs (Seto *et al.*, 2011a) and, most notably, early identification of a phototoxic potential for new drug entities (Onoue *et al.*, 2009). Strategic screening for photosafety is necessary at the early phase of the drug discovery process and even before introducing drugs into clinical therapy, as rapid and reliable photosafety evaluation would be of great help for the prevention of unwanted drug reactions in humans. Therefore, a number of assay systems have been designed for the assessment of photosensitive/phototoxic potential through analytical and biochemical methods (Onoue *et al.*, 2009; Seto *et al.*, 2012).

According to the first law of photochemistry, the primary event in any photochemical and/or photobiochemical process is the absorption of photon energy, followed by the generation of reactive oxygen species (ROS). From a theoretical standpoint, the ROS assay was developed for *in vitro* photoreactivity and phototoxicity assessment, in which the generation of singlet oxygen and superoxide anion from photo-activated chemicals is quantitatively determined (Onoue and Tsuda, 2006; Onoue *et al.*, 2008a). The good relationship between ROS data and *in vivo* phototoxicity revealed the prediction capacity of the ROS assay; however, through multi-laboratory validation study, there appeared to be two assay limitations, namely (i) false-positive predictions and (ii) solubility issues (Onoue *et al.*, 2012). The ROS assay is commonly used for early photosafety evaluation with appropriate follow-up assessments, so the former issue may not always be problematic as long as chemicals are not falsely predicted as non-phototoxic. In contrast, experimental problems arising from the limited solubility have a major impact on assay performance and applicability. In such cases, appropriate options to modify the ROS assay system would be required for reliable photosafety assessment on poorly water-soluble chemicals.

**Correspondence to: Satomi Onoue, Department of Pharmacokinetics and Pharmacodynamics, School of Pharmaceutical Sciences, University of Shizuoka, 52-1 Yada, Suruga-ku, Shizuoka 422-8526, Japan. E-mail: onoue@u-shizuoka-ken.ac.jp*

Department of Pharmacokinetics and Pharmacodynamics, School of Pharmaceutical Sciences, University of Shizuoka, 52-1 Yada, Suruga-ku, Shizuoka 422-8526, Japan

In the present study, to overcome these limitations, a modified ROS assay system was newly developed using bovine serum albumin (BSA) for two major reasons: (i) co-existing albumin might provide an experimental biomimetic environment to some extent as some chemicals tend to interact with albumin, and (ii) albumin could also act as a potent solubilizer for poorly water-soluble drugs (Kurono *et al.*, 1987). Determination of ROS in an albuminous solution might partly reflect the photochemical behavior of photosensitizers *in vivo*, and the albuminous ROS (aROS) assay system might be more effective for photosafety evaluation with fewer false predictions. In this study, 21 phototoxins and 10 non-phototoxic chemicals were assessed by both ROS and aROS assays to clarify the prediction capacity of these assay systems. The precision of the aROS assay was also assessed by repeated measurement and calculation of the Z'-factor, a characteristic parameter reflecting the quality of the assay. In addition, spectroscopic experiments were carried out to evaluate the possible interaction of photosensitizing compounds with albumin by UV and fluorescent spectrometry.

Materials and Methods

Chemicals

According to the reported *in vitro/in vivo* photosafety information and clinical observations (Alvarez-Fernandez *et al.*, 2000; Lim and Hawk, 2008; Onoue *et al.*, 2012; Quintero and Miranda, 2000; Selvaag, 1997; Seto *et al.*, 2011b), 2 standard chemicals and 29 test chemicals, including 20 phototoxins and 9 non-phototoxic drugs/chemicals, were selected as model chemicals for the present study (Table 1).

Quinine HCl (**1**), chlorpromazine HCl (**6**), glibenclamide (**8**), gliclazide (**9**), glimepiride (**10**), griseofulvin (**11**), norfloxacin (**16**), ofloxacin (**17**), piroxicam (**18**), promethazine HCl (**19**), quinidine H_2SO_4 $2H_2O$ (**20**), aspirin (**23**), benzocaine (**24**), erythromycin (**25**), *para*-aminobenzoic acid (PABA, **27**), penicillin G (**28**), phenytoin (**29**), sodium dodecyl sulfate (SDS, **30**), warfarin Na (**31**), NaH_2PO_4 $2H_2O$, Na_2HPO_4 $12H_2O$, dimethyl sulfoxide (DMSO), *p*-nitrosodimethylaniline, imidazole and nitroblue tetrazolium (NBT) were obtained from

Table 1. Outcomes from reactive oxygen species (ROS) and albuminous reactive oxygen species (aROS) assays on known phototoxins and non-phototoxic chemicals

No.	Chemical name	CAS No.	Form	Singlet oxygen ($\Delta A_{440\,nm} \cdot 10^3$)		Superoxide ($\Delta A_{560\,nm} \cdot 10^3$)		Photosafety information	
				ROS assay	aROS assay	ROS assay	aROS assay	Phototoxicity	Photoallergy
Positive/Negative controls									
1	Quinine HCl	6119-47-7	Solid	519±8	455±7	398±3	617±7	+ a	
2	Sulisobenzone	4065-45-6	Solid	-1±1	-70±5	-19±1	4±35	− a	
Phototoxic chemicals									
3	6-Methylcoumarin	92-48-8	Solid	148±34	126±11	108±15	12±2	+ a	+ b
4	Bithionol	97-18-7	Solid	39±9	-3±14	14±2	43±9	+ a	+ b
5	Chlorhexidine	55-56-1	Solid	-5±0	-27±3	23±1	49±2	+ a	+ b
6	Chlorpromazine HCl	69-09-0	Solid	-11±12	48±20	63±9	65±2	+ a	+ b
7	Diclofenac Na	15307-79-6	Solid	311±2	80±30	403±14	-13±1	+ a	+ b
8	Glibenclamide	10238-21-8	Solid	5±12	35±6	12±7	57±0	+ d	
9	Gliclazide	21187-98-4	Solid	-1±4	-70±5	225±3	165±7	+ d	
10	Glimepiride	93479-97-1	Solid	-13±4	0±3	41±13	38±1	+ e	
11	Griseofulvin	126-07-8	Solid	22±10	-18±5	27±6	-2±2	+ a	+ b
12	Hexachlorophene	70-30-4	Solid	266±4	-10±8	-25±15	10±6	+ a	+ b
13	Itraconazole	84625-61-6	Solid	86±4	35±4	-11±9	28±1	+ c	+ c
14	Ketoprofen	22071-15-4	Solid	301±8	336±16	112±7	66±1	+ a	+ b
15	Lomefloxacin HCl	98079-52-8	Solid	603±3	355±15	82±6	36±4	+ f	+ b
16	Norfloxacin	70458-96-7	Solid	179±18	238±17	100±2	41±2	+ a	+ b
17	Ofloxacin	82419-36-1	Solid	169±15	328±21	416±14	524±23	+ d	+ b
18	Piroxicam	36322-90-4	Solid	166±11	358±3	103±6	456±10	+ a	+ b
19	Promethazine HCl	58-33-3	Solid	73±4	175±34	56±3	93±4	+ a	+ b
20	Quinidine H_2SO_4 $2H_2O$	6591-63-5	Solid	592±26	408±4	405±19	555±2	+ a	+ b
21	Tetracycline	60-54-8	Solid	221±12	105±8	200±2	211±4	+ a	+ b
22	Tolbutamide	64-77-7	Solid	-9±13	3±6	44±6	50±3	+ d	
Non-phototoxic chemicals									
23	Aspirin	50-78-2	Solid	4±12	-2±45	25±26	-13±8	− a	
24	Benzocaine	94-09-7	Solid	-9±6	-88±3	3±16	-7±16	− a	
25	Erythromycin	114-07-8	Solid	-29±10	-12±8	6±5	-4±2	− a	
26	Octyl methoxycinnamate	5466-77-3	Solid	11±9	-52±3	-1±11	17±2	− a	
27	PABA	150-13-0	Solid	-17±16	-17±17	-16±10	-5±10	− a	
28	Penicillin G	113-98-4	Solid	14±9	3±19	46±22	-6±1	− a	
29	Phenytoin	57-41-0	Solid	-28±23	-13±33	17±26	-8±4	− a	
30	SDS	151-21-3	Solid	7±4	17±20	3±2	-14±8	− a	
31	Warfarin Na	129-06-6	Solid	7±1	-69±25	55±1	-19±10	− a	

ROS and aROS assays were basically carried out for test chemicals at a concentration of 200 μM, and data on the diluted chemicals are boxed (100 μM) or emphasized with gray (50 μM) and black (20 μM). References: a, (Onoue *et al.*, 2012); b, (Lim and Hawk, 2008); c, (Selvaag, 1997); d, (Quintero & Miranda, 2000); and e, (Seto *et al.*, 2011b).

Table 2. Intra- and inter-day (days 1 and 3) precision for reactive oxygen species (ROS) of irradiated quinine HCl (200 μM) in the presence of bovine serum albumin (BSA)

	Generation of reactive oxygen species, mean ± SD (%RSD)	
	Singlet oxygen (Decrease of $A_{440\ nm} \times 10^3$)	Superoxide (Increase of $A_{560\ nm} \times 10^3$)
Intra-day	435 ± 10.6 (2.4)	576 ± 21.6 (3.8)
Inter-day	436 ± 9.1 (2.1)	592 ± 7.6 (1.3)

Data represent mean ± standard deviation (SD) of 5 experiments for intra-day precision and 10 experiments for inter-day precision.

Wako Pure Chemical Industries (Osaka, Japan). Sulisobenzone (**2**), bithionol (**4**), hexachlorophene (**12**), ketoprofen (**14**) and octyl methoxycinnamate (**26**) were purchased from Tokyo Chemical Industry (Tokyo, Japan). 6-Methylcoumarin (**3**), chlorhexidine (**5**), diclofenac Na (**7**), lomefloxacin HCl (**15**), tetracycline (**21**), tolbutamide (**22**) and bovine serum albumin (BSA) were purchased from Sigma-Aldrich Japan (Tokyo, Japan). Itraconazole (**13**) was bought from LKT Laboratories (St. Paul, MN, USA). A quartz reaction container for a high-throughput ROS assay (Onoue *et al.*, 2008a) was constructed by Ozawa Science (Aichi, Japan).

Irradiation

The ROS and aROS assays were conducted using Atlas Suntest CPS plus (Atlas Material Technology LLC, Chicago, USA) equipped with a xenon arc lamp (1500 W). A UV special filter was installed to adapt the spectrum of the artificial light source to that of natural daylight, and the Atlas Suntest CPS series had a high irradiance capability that met CIE85/1989 daylight simulation requirements. The irradiation test was carried out at 25 °C with an irradiance of *c.* 2.0 mW/cm^2 as determined by the calibrated UVA detector Dr Hönle no. 0037 (Dr Hönle, München, Germany).

ROS Assay Procedure

The ROS assay was designed to detect both singlet oxygen and superoxide generated from photo-irradiated chemicals (Onoue *et al.*, 2008a, 2008b). Briefly, singlet oxygen was measured in an aqueous solution by spectrophotometrically monitoring the bleaching of *p*-nitrosodimethylaniline at 440 nm using imidazole as a selective acceptor of singlet oxygen. Samples, containing the tested chemical (20–200 μM), *p*-nitrosodimethylaniline (50 μM), and imidazole (50 μM) in 20 mM sodium phosphate buffer (NaPB, pH 7.4), were mixed in a tube. For the aROS assay, BSA at a concentration equal to that of the tested chemical was added to the reaction mixture. Two hundred microliters of the sample was transferred into a well of a plastic 96-well plate (clear, untreated, flat-bottomed; Asahi Glass Co., Ltd., Tokyo, Japan) and checked for precipitation before light exposure. The plate was subjected to measurement of absorbance at 440 nm using a SAFIRE microplate spectrophotometer (TECAN, Mannedorf, Switzerland). The plate was fixed in the quartz reaction container with a quartz cover, and then irradiated with the simulated sunlight for 1 h. After agitation on a plate shaker, the UV absorbance at 440 nm was measured. For the determination of superoxide, samples containing the tested chemical (20–200 μM), NBT (50 μM), and/or BSA (20–200 μM) in 20 mM NaPB were irradiated with the simulated sunlight for 1 h, and the reduction in NBT was measured by the increase in absorbance at 560 nm in the same manner as the singlet oxygen determination. Experiments were performed in triplicate wells in three independent runs. As the final concentration, 200 μM of the test chemical solutions should have been subjected to the ROS assay. However, when precipitation could be observed at 200 μM under an optical microscope, additional experiments were performed at 20, 50, or 100 μM. When precipitation was observed at 20 μM in the reaction mixture, no further experiment was carried out.

Criteria for Data Acceptance and Judgment

According to the result (mean of triplicate determinations) from the ROS assay, photoreactivity on each test chemical should be judged to be (i) positive with singlet oxygen ($\Delta A_{440\ nm} \times 10^3$): 25 or more; and/or superoxide ($\Delta A_{560\ nm} \times 10^3$): 20 or more, or (ii) negative with singlet oxygen: less than 25 ($\Delta A_{440\ nm} \times 10^3$) and superoxide ($\Delta A_{560\ nm} \times 10^3$): less than 20. The final decision should be made as follows: (i) positive: above the threshold level for singlet oxygen or superoxide; or (ii) negative: below the threshold level for both singlet oxygen and superoxide.

These criteria were defined for the ROS assay on tested chemicals at a concentration of 200 μM, and, therefore, they would not be theoretically applicable to the outcomes from assays at a lower concentration (< 200 μM). However, the tested chemicals could be identified to be phototoxic as long as the ROS data at a lower concentration (< 200 μM) surpassed these tentative classification criteria, so that these criteria might still be available for a positive prediction on the diluted samples. In contrast, it would be challenging to make negative predictions on the basis of a ROS assay under dilution.

Z'-factor

To evaluate the robustness of the aROS assay, the Z'-factor, a statistical function, was calculated using the following equation: $Z' = 1 - (3\sigma_{c+} + 3\sigma_{c-})/|\mu_{c+} - \mu_{c-}|$ (Zhang *et al.*, 1999). The means of the positive and negative control signals are denoted as μ_{c+} and μ_{c-}, respectively. The SDs of the signals are denoted as σ_{c+} and σ_{c-}, respectively. The difference between the means, $|\mu_{c+} - \mu_{c-}|$, defines the assay dynamic range.

Solubility Test

Equilibrium solubility of glibenclamide (**8**) was measured as follows: an excessive amount of glibenclamide (**8**) was added to the reaction mixture for superoxide with or without 200 μM of BSA to keep the concentration constant at 1 mg ml^{-1}. Samples were put in a shaker and shaken for 48 h at 25 °C. The samples were centrifuged at 15 000 *g* for 5 min, and the supernatant was mixed with a threefold volume of acetonitrile and then centrifuged at 10 000 *g* for 5 min. The concentration of dissolved glibenclamide (**8**) in the supernatant was determined by Waters Acquity UPLC system (Waters, Milford, MA, USA), which included a binary solvent manager, sample manager, column compartment and a SQD connected with MassLynx software. An Acquity UPLC BEH C 18 column (particle size: 1.7 μm, column size: 2.1 × 50 mm; Waters) was used, and column temperature was maintained at 40 °C. Samples were separated using a gradient mobile phase consisting of acetonitrile (A) and 0.1% formic acid (B) with a flow rate of 0.25 ml min^{-1}, and the retention time of glibenclamide (**8**) was 2.4 min. The gradient condition of the mobile phase was 0–1.0 min, 50% A; 1.0–4.0 min, 50–95% A; and 4.0–5.0 min, 95% A. Analysis was carried out using selected ion recording (SIR) for specific *m/z* 495 for glibenclamide (**8**) $[M+H]^+$.

UV Spectral Analysis

Chemicals were dissolved in 20 mM sodium phosphate buffer (NaPB, pH 7.4) at a final concentration of 20 μM. UV/VIS absorption spectra were recorded with a Hitachi U-2010 spectrophotometer (Hitachi High-Technologies Corporation, Tokyo, Japan) interfaced to a PC for data processing (software: Spectra Manager). A spectrofluorimeter quartz cell with 10-mm path length was employed.

Fluorescence Quenching Assay

To ensure a molecular interaction between serum albumin and the tested chemical, a fluorescence quenching assay was carried out according to a previous report with some modifications (Fukuhara *et al.*, 2012). Each tested chemical and/or BSA were dissolved in 20 mM NaPB (pH 7.4) at a final concentration of 2 μM. After incubation at 25 °C for 30 min, the intrinsic tryptophan fluorescence in BSA solution with or without tested chemical was measured using a SAFIRE microplate spectrophotometer (TECAN) with an excitation wavelength of 295 nm and an emission wavelength of 340 nm.

Results and Discussion

ROS Generation from Quinine HCl with or without BSA

Serum albumin is the most abundant protein in plasma, accounting for *c.* 60% of its total protein content and providing *c.* 80% of the blood osmotic pressure (Carter and Ho, 1994). Considerable attention has also been drawn to the biological functions of serum albumin for drug transport and storage in vertebrates through the formation of non-covalent binding. Therefore, even although the condition in the presence of albumin might not be accurately biomimetic, serum albumin has been widely used to provide experimental biomimetic conditions in assay development (Andrade and Costa, 2008; Danel *et al.*, 2006). The interaction of albumin with a poorly water-soluble chemical also led to an improvement in its solubility; therefore, the use of albumin for the ROS assay would offer biomimetic experimental conditions partly and solubility enhancement. To verify the feasibility of the aROS assay, ROS and aROS assays were carried out for two standard chemicals, quinine HCl (**1**), a typical phototoxin (Moore, 2002), and sulisobenzone (**2**), a non-phototoxic chemical (Portes *et al.*, 2002). In the ROS assay (Table 1), quinine HCl (**1**: 200 μM) generated both singlet oxygen and superoxide when exposed to the simulated sunlight (*c.* 2.0 mW/cm^2) for 1 h, whereas ROS generation was negligible from irradiated sulisobenzone (**2**: 200 μM). Both standards did not exhibit any ROS generation under light protection (data not shown). Similar photochemical responses on these standards were also observed in the aROS assay, whereas the addition of equimolar albumin into quinine HCl (**1**: 200 μM) resulted in transition of the generated ROS, as evidenced by *c.* 12% decrease in singlet oxygen and *c.* 55% increase in superoxide. These findings were partly in agreement with a previous observation, showing that non-covalently bound serum albumin modulated the photochemical behavior of a bacteriochlorophyll derivative (Ashur *et al.*, 2009). It would be highly challenging to mimic the physiological environment exactly; however, aROS data on quinine HCl (**1**) might partly reflect the *in vivo* photochemical behavior upon interaction with serum albumin.

To assess the robustness and reproducibility of the aROS assay, the Z′-factor was also calculated according to the method of Zhang *et al.* (1999). The Z′-factor is designed to reflect both the assay signal noise ratio and the variation associated with the signal measurements. Hence, the Z′-factor is commonly utilized for quality assessment in assay development and optimization, as well as evaluation of the reproducibility of assays used for high-throughput screening campaigns (Rega *et al.*, 2007). The Z′-factor is close to 1.0 in an ideal assay, and a Z′-factor greater than 0.5 is indicative of an excellent assay, whereas assays with Z′ values less than 0.5 show a small separation band. Typical values from multiple measurements (21 times) of quinine HCl (**1**: 200 μM) and sulisobenzone (**2**: 200 μM) are shown in Fig. 1A (singlet oxygen) and 1B (superoxide). The Z′-factors for the determination of singlet oxygen and superoxide were calculated to be 0.93 and 0.79, respectively, demonstrating that the assay allows a large separation band between samples and blank signals and thereby confirming its suitability for high-throughput screening. The overall precision of the aROS assay was also evaluated by analyzing nine samples of quinine HCl (**1**) solution at 200 μM (Table 2). The intra-day coefficients of variation (CV) for the detection of singlet oxygen and superoxide generated from irradiated quinine HCl (**1**) were found to be 2.4% and 3.8%, respectively. In addition, the inter-day CV values for quinine HCl (**1**) were calculated to be 2.1% for singlet oxygen and 1.3% for superoxide. Thus, the CV value obtained was below 4%, showing that the proposed analytical method has good intra- and inter-day precision.

Prediction Capacity of Albuminous ROS Assay

To evaluate the predictive capacity of an aROS assay, in addition to 2 standard chemicals (**1** and **2**), 29 chemicals, consisting of 20 known phototoxins (**3–22**) and 9 non-phototoxic drugs/chemicals (**23–31**), were also assessed by the ROS and aROS assays (Table 1 and Fig. 2).

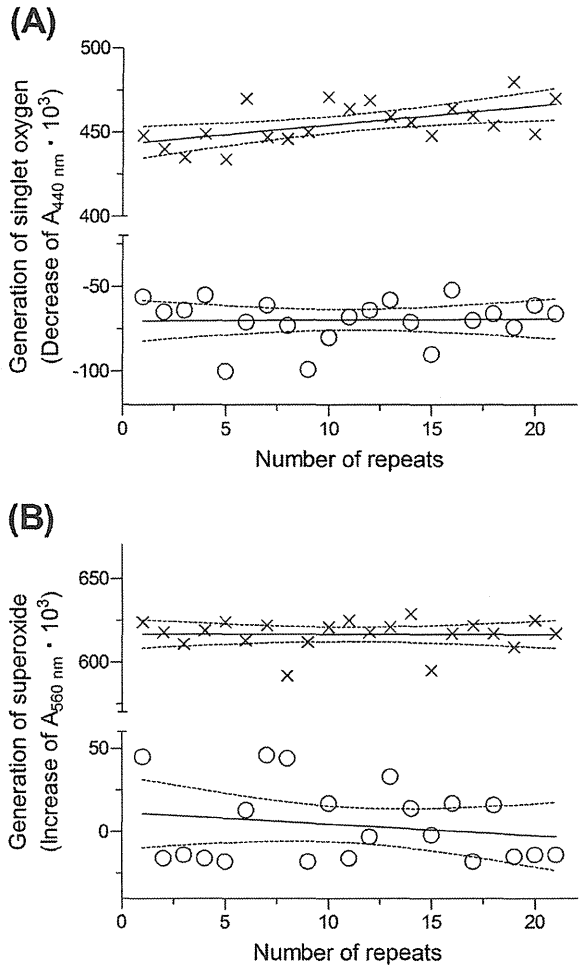

Figure 1. Representative multiple measurement data used to calculate the Z'-factor for the albuminous reactive oxygen species (aROM) assay. Quinine HCl as a positive control (×) or sulisobenzone as a negative control (○) at a concentration of 200 μM was dissolved in 20 mM sodium phosphate buffer (pH7.4) and exposed to simulated sunlight (2.0 mW/cm^2) for 60 min. Generation of (A) singlet oxygen and (B) superoxide was determined. Lines indicate mean ± 95% confidence interval.

For the ROS assay, 26 chemicals (84% of the total) could be assessed at the concentration of 200 μM, and 5 chemicals had to be diluted to a final concentration of 20, 50 or 100 μM because of limited solubility in aqueous media. Most phototoxins even under dilution demonstrated potent ability to generate singlet oxygen, superoxide, or both under UV/VIS exposure (Fig. 2A). In contrast, ROS generation from most non-phototoxic chemicals was negligible, except for aspirin (**23**), penicillin G (**28**) and warfarin Na (**31**). According to the threshold values [25 for singlet oxygen ($\Delta A_{440\ nm} \times 10^3$) and 20 for superoxide anion ($\Delta A_{560\ nm} \times 10^3$)] defined for the ROS data at 200 μM, most phototoxins tested here were correctly identified to be phototoxic by the ROS assay, whereas only glibenclamide (**8**) was unevaluable because of its poor solubility. Of all 10 non-phototoxic chemicals, 5 compounds (**2**, **24**, **25**, **27** and **29**) were found to be non-phototoxic on the basis of ROS data at 200 μM, and the negativity for 2 chemicals (**26** and **30**) could not be fully proven as they were assessed at a lower concentration. Thus, some

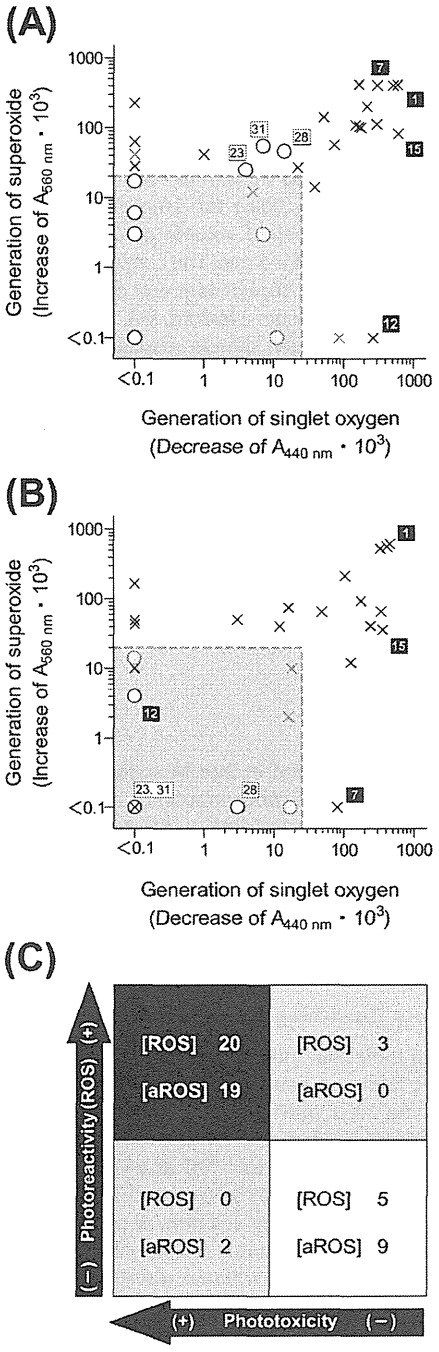

Figure 2. Predictive capacity of the albuminous reactive oxygen species (aROS) assay. Plot of singlet oxygen data versus superoxide data for all tested chemicals obtained from the ROS assay (A) and aROS assay (B). ○, non-phototoxic chemicals; and ×, phototoxins at concentrations of 20–100 (red symbols) and 200 μM (black symbols). Symbols with a number represent the data on quinine HCl (**1**), diclofenac Na (**7**), hexachlorophene (**12**), lomefloxacin HCl (**15**), aspirin (**23**), penicillin G (**28**) and warfarin Na (**31**). Each value represents the mean of three experiments. According to the criteria for phototoxins (200 μM) defined previously, the shaded region is indicative of low phototoxic potential. (C) Positive and negative predictivity of the ROS and aROS assays as compared with the *in vitro/in vivo* phototoxicity.